University of Baghdad
College of Engineering
JOURNAL OF ENGINEERING

Journal of Engineering

journal homepage: www.jcoeng.edu.iq

Volume 32 Number 9 September 2026

Finite Element Analysis of the Flexural Performance of Hybrid (Steel-BFRP) RC Beams under Repeated Loading: Verification and Parametric Investigation

Shahad Jawad Kadhim*, **Hassan Falah Hassan**

Civil Engineering Department, College of Engineering, Mustansiriyah University, Baghdad, Iraq

ABSTRACT

The corrosion of steel bars in reinforced concrete structures subjected to harsh environments remains a significant challenge. Fiber-reinforced polymer (FRP) composites have been investigated as potential alternatives to conventional steel reinforcement. While basalt fiber-reinforced polymer (BFRP) bars exhibit high tensile strength, durability, and sustainability, they are characterized by linear elastic behavior and a brittle failure mode. Hybrid reinforcements of steel and BFRP bars combine the ductility of steel with the corrosion resistance of BFRP. This study presents the development and validation of a three-dimensional nonlinear finite element (FE) model in ABAQUS to simulate the flexural behavior of high-strength concrete (HSC) beams reinforced with a hybrid (steel/BFRP) system under repeated loading. Six beam specimens with a compressive strength of 86.5 MPa were modeled and validated against experimental results. The FE model predicted ultimate load capacity with an average error of 4.97%, while deflection predictions showed an average error of 17.44%. The beams failed when the concrete cracked before the BFRP bars reached their full tensile capacity. A parametric study investigated the effects of increasing the concrete compressive strength from 86.5 MPa to 120 MPa on BFRP stress utilization, ultimate load capacity, and failure mode. Numerical results predict that increasing the concrete strength to 120 MPa significantly enhances structural performance, suggesting a shift in failure mode as indicated by the model. These findings provide valuable insights into optimizing hybrid reinforcement systems for improved structural efficiency and durability.

Keywords: HSC beams, Hybrid reinforcement, Repeated loading, ABAQUS, Validation, Parametric study.

1. INTRODUCTION

For over a century, reinforced concrete (RC) was the most widely used building material because of its flexibility, strength, and durability **(Maheswaran and Chellapandian, 2023;**

*Corresponding author
Peer review under the responsibility of University of Baghdad.
https://doi.org/10.31026/j.eng.2026.09.05

Article received: 26/05/2026
Article revised: 23/07/2026
Article accepted: 08/08/2026
Article published: 01/09/2026

Kossakowski and Wciślik, 2022). However, traditional steel-reinforced concrete structures are highly susceptible to chloride ingress, carbonation, freeze-thaw cycles, and have failed because of corrosion of the steel reinforcement, which results in cracking, spalling, and eventually failing **(Maheswaran and Chellapandian, 2023; Oyshi et al., 2023)**. Corromination of steel is one of the most expensive repairs, restoration, and replacement costs for annual costs totaling billions of dollars **(Ineia et al., 2021; Maheswaran and Chellapandian, 2023)**. These effects of corrosion on infrastructure have led researchers to looking for other reinforcement materials that can withstand corrosion and structural integrity **(Tatar and Milev, 2021; Ortiz et al., 2023).** Fiber-reinforced polymer (FRP) composites are a good alternative to steel reinforcement due to their corrosion resistance, high strength-to-weight ratio, and durability in aggressive environments **(ACI Committee 440, 2015; Ren et al., 2023).** Glass FRP, carbon FRP, and basalt FRP have also received attention. Basalt is a volcanic rock that provides high tensile strength, chemical resistance, thermal stability, and environmental sustainability **(Mohamed et al., 2021)**. However, research findings on the efficacy of BFRP are not entirely uniform. For instance, Although **(Abed et al., 2021)** noted significant improvements in cracking and ultimate moments of 10% and 16% respectively, **(Al-Zahrani et al., 2023)** shows that the structural gains occur primarily due to the strength of concrete. These studies may have been misleading because they are monotonic and therefore fail to account for sudden and fragile failure characteristic of FRP-reinforced members **(Hollaway and Teng, 2008)**. For this reason, hybridization (combining steel and FRP) was introduced **(Rasheed et al., 2004; Nguyen et al., 2020)**. High-strength concrete has also been recommended by the American Concrete Institute **(ACI Committee 440, 2015)** and should be used with FRP. Recently, **(Xie et al., 2022)** reported that reactive powder concrete (RPC) can exhibit plastic behavior in BFRP systems. Yet, **(Salem and Issa, 2023)** showed that the interaction between concrete strength and type of reinforcement can vary greatly depending on stress stage. Despite these findings, most hybrid studies still involve normal-strength concrete. Few studies explore the degradation of these systems under repeated loading cycles.

From a numerical perspective, The Concrete Damaged Plasticity (CDP) model in ABAQUS is a well-known tool for simulating nonlinear behavior **(Bažant and Jirásek, 2002; Abaqus Documentation)**, but its application to hybrid Steel-BFRP beams made of high-strength concrete (HSC) is still in its infancy. Recent works by **(Abdulrahman, 2025; Assi, 2025)** have provided localized information on the crack prediction of RC beams and ductility improvement in RC beams. Further literature **(Al-Shaarbaf et al., 2017; Yan and Wang, 2025)** has validated numerical models for deep beams and hybrid bolt connections respectively. While numerical models for FRP-reinforced or hybrid steel/FRPbeams exist, there has been no research on the use of hybrid Steel-BFRP reinforcement in HSC members with multiple cycles of load in the ABAQUS Concrete Damaged Plasticity (CDP). Recent studies have emphasized the potential of hybrid steel-FRP systems; however, traditional design codes such as **(ACI Committee 440, 2015)** often provide conservative estimates as they primarily focus on monotonic behavior and do not fully account for the synergistic interaction between steel and BFRP bars in high-strength matrices **(Megahed, 2025; Elbawab et al., 2025).** Further, the current design formulas for deflection and crack width are mostly for normal-strength concrete, which may yield inaccurate predictions for HSC members with repeated loading cycles. Numerical simulations such as ABAQUS can provide a better understanding of the emergence of damage and redistribution of stress in these complex systems. Plus, there are no parametric studies investigating the effect of concrete compressive strength on use of BFRP stress and failure mode in hybrid structures. This is an important connection to consider when designing hybrid reinforced concrete and how best use BFRP tensile strength. The purposes of this research were to validate a three-dimensional nonlinear finite element model developed using ABAQUS for the flexural behavior of hybrid steel/BFRP reinforced high-strength concrete beams, and to evaluate the effect of increasing the concrete compressive strength from 86.5 MPa to 120 MPa on the use of BFRP stress, ultimate load, and failure mode. Both model and parametric results are important for structural engineers and researchers studying the durability of high-performance concrete structures with hybrid reinforcement.

2. EXPERIMENTAL PROGRAM

2.1 Beam Details and Reinforcement Configurations

The experimental program comprised six geometrically identical reinforced concrete beams subjected to a four-point bending configuration under repeated loading. Each beam was 2000 mm in length and span 1800 mm between the supports, with a rectangular cross-section of 150 mm in width and 250 mm in depth and covered in clear concrete with 20 mm. **Fig. 1** displays the details and dimensions of the beams. The beams had systematically different configurations of reinforcement to investigate the effects of the steel/BFRP ratios on strength. All longitudinal reinforcing bars, both steel and BFRP, had a nominal diameter of 10 mm to ensure consistency in bond strength and to avoid the effects of type of material on its bonding.

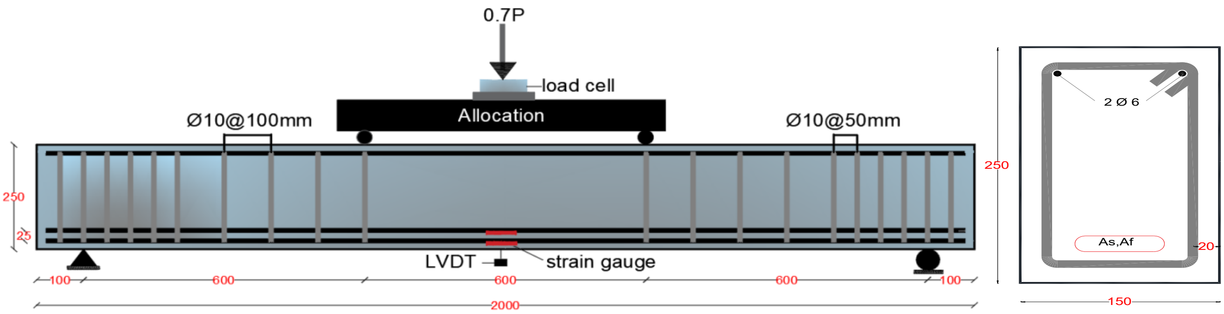

Figure 1. Details and dimensions of beams (all dimensions in mm)

Beam designations and the details of the reinforcement are described in **Table 1.** The control beam (6S) was reinforced entirely with six steel bars in the tension zone to establish a reference case. Beam (6B) was reinforced entirely with BFRP bars to evaluate the behavior of a fully FRP-reinforced member. The remaining beams (2B-4S, 3B-3S, 4B-2S, 5B-1S) incorporated hybrid steel/BFRP reinforcement systems with increasing BFRP content. All beams were provided with shear reinforcement in the form of closed stirrups with a diameter of 10 mm to prevent shear failure and ensure that flexural behavior governed the response. The spacing of the stirrups was 100 mm near the loading points and reduced to 50 mm toward the supports. The constant moment region between the loading points was left without stirrups to ensure flexure-dominated behavior and facilitate clear observation of flexural crack development. Compression reinforcement consisted of two 6 mm steel bars to maintain cage stability. Beam notation follows the format (No-Reinf) for non-hybrid beams and (No-Reinf-No-Reinf) for hybrid beams, where (No) represents the number of reinforcement bars in the beam, and (Reinf) represents the type of longitudinal reinforcement (B for Basalt fiber-reinforced polymer (BFRP) and S for steel).

Table 1. Details of beam specimens and reinforcement configurations

(6S) 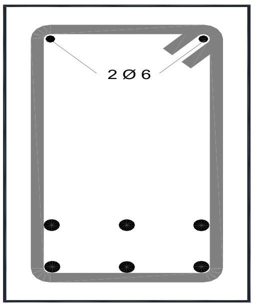 = 460 mm^2 $\boldsymbol{A_s}$ = 1.55% $\boldsymbol{\rho_s}$	**(2B)** 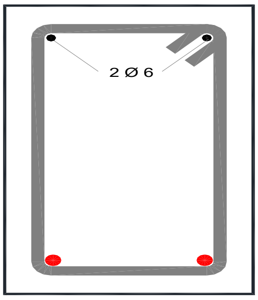 = 142.4 mm^2 $\boldsymbol{A_f}$ = 0.44% $\boldsymbol{\rho_f}$	**(3B)** 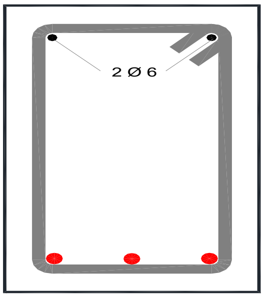 = 213.6 mm^2 $\boldsymbol{A_f}$ = 0.66% $\boldsymbol{\rho_f}$
(4B) 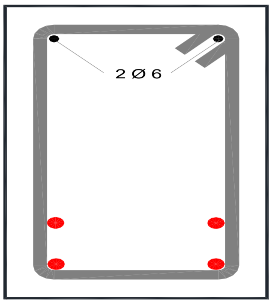 = 284.8 mm^2 $\boldsymbol{A_f}$ = 0.96% $\boldsymbol{\rho_f}$	**(6B)** 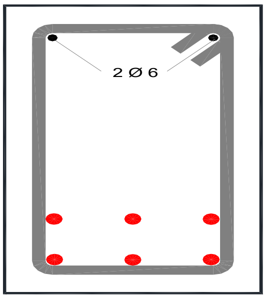 = 427.2 mm^2 $\boldsymbol{A_f}$ = 1.44% $\boldsymbol{\rho_f}$	**(2B-4S)** 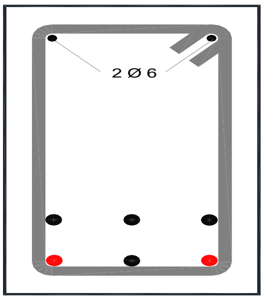 = 306.6 mm^2 $\boldsymbol{A_s}$ = 1.04% $\boldsymbol{\rho_s}$ = 142.4 mm^2 $\boldsymbol{A_f}$ = 0.48% $\boldsymbol{\rho_f}$
(3B-3S) 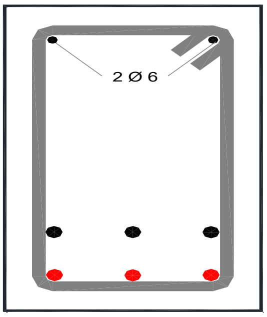 = 230 mm^2 $\boldsymbol{A_s}$ = 0.78% $\boldsymbol{\rho_s}$ = 213.6 mm^2 $\boldsymbol{A_f}$ = 0.72% $\boldsymbol{\rho_f}$	**(4B-2S)** 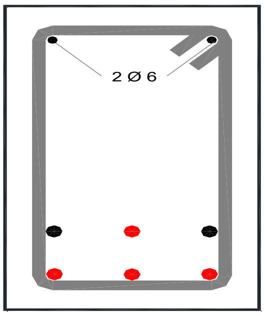 = 153.3 mm^2 $\boldsymbol{A_s}$ = 0.52% $\boldsymbol{\rho_s}$ = 284.8 mm^2 $\boldsymbol{A_f}$ = 0.96 $\boldsymbol{\rho_f}$	**(5B-1S)** 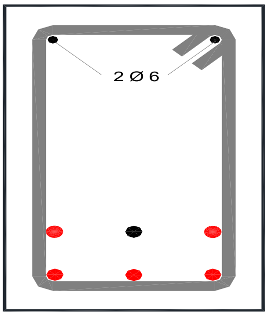 = 76.6 mm^2 $\boldsymbol{A_s}$ = 0.26% $\boldsymbol{\rho_s}$ = 356.5 mm^2 $\boldsymbol{A_f}$ = 1.20% $\boldsymbol{\rho_f}$

Note: * A_s and A_f are the area of steel and BFRP bars respectively; ρ_s and ρ_f are the steel and BFRP reinforcement ratio.
*Top Reinforcement Type = 2Ø6mm steel for all beams.
* ● STEEL ● BFRP

2.2 Concrete Mix Design

High-strength concrete (HSC) was used for all specimens. The high-strength concrete mix was proportioned based on the guidelines of ACI 211.4R-08 (Guide for Selecting Proportions for High-Strength Concrete), utilizing silica fume and a low water-to-binder ratio to achieve the target strength **(ACI Committee 211, 2008)**. The mix proportions based **(Aziz and**

Hassan, 2025) and are presented in **Table 2.** Ordinary Portland cement (Type I) was used in combination with silica fumes to improve strength and durability. Silica fume, which complies with **(ASTM C1240, 2015)**, functions as a pozzolanic material that fills voids in the cement paste, refines the pore structure, and decreases permeability through its pozzolanic reaction with calcium hydroxide **(Thomas, 2013)**. A high-range water-reducing admixture (superplasticizer) that meets the specifications of **(ASTM C494/C494M, 2019)** Type F was incorporated to achieve the required workability while preserving a low water-to-cement ratio of 0.22. The concrete mix was prepared using a laboratory mixer. Standard (100 × 200) mm cylindrical specimens were cast alongside the beams for compressive strength evaluation. The average compressive strength at 28 days was 86.5 MPa.

Table 2. Concrete mixture proportions

Cement (Kg/m^3)	**Sand (Kg/m^3)**	**Gravel (Kg/m^3)**	**Silica fume (Kg/m^3)**	**Superplasticizer (Kg/m^3)**	**Water L/m^3**	**W/C ratio**
650	800	650	110	26	143	0.22

2.3 Material Properties

Steel and BFRP bars with a nominal diameter of 10 mm were used. **Table 3** presents the mechanical properties of both materials.

Table 3. Mechanical Properties of Steel and BFRP reinforcement

Type of reinforcement	**Nominal Diameter (mm)**	**Yield Strength (MPa)**	**Maximum tensile strength (Mpa)**	**Modulus of Elasticity (Gpa)**
Steel	10	445	667	200
BFRP	10	/	950	55

2.4 Loading Protocol

All beams were tested under a four-point bending configuration, producing a constant moment region between the two loading points. The beams were simply supported over a span of 1800 mm, with two equal loads applied symmetrically at 600 mm from each support, creating a constant moment region of 600 mm between the loading points as shown in **Fig. 1**. The loading protocol consisted of two phases: a repeated loading phase and a monotonic loading to failure phase. In the repeated loading stage, all beams were subjected to a repeated loading where, the target of maximum load level at each cycle was 70% of the ultimate static flexural capacity of each beam according to **(ACI Committe 440, 2015)**, in addition to recent experimental studies **(Alkhteeb and Dawood, 2025)**, which recorded by **(Aziz and Hassan, 2025)**, followed by unloading to zero load. The beams were loaded for a different number of cycles depending on the deflection when it reached (70-80) % of the maximum static deflection determined from preliminary static test, the loading was terminated (all beams reached the same damage). Following the completion of the repeated loading phase, each beam was subjected to monotonic loading to failure to determine the residual capacity and failure mode.

3. FINITE ELEMENT MODELING

3.1 General Modeling Approach

A three-dimensional nonlinear finite element model was developed using ABAQUS/Standard 2022 to simulate the flexural response of hybrid steel/BFRP reinforced high-strength concrete beams subjected to repeated loading. ABAQUS/Standard employs an implicit integration scheme that is well-suited for quasi-static problems involving material nonlinearity, contact, and complex boundary conditions (Abaqus Documentation). The main parts of the finite element model include (1) concrete beam body, (2) longitudinal reinforcement (steel or BFRP bars for bottom and steel for top), (3) transverse shear reinforcement, and (4) steel loading/support plates. Each component was modeled with appropriate element types, material constitutive models, and interaction properties to accurately represent the physical behavior observed in experiments. **Fig. 2** presents the details of the concrete beam model.

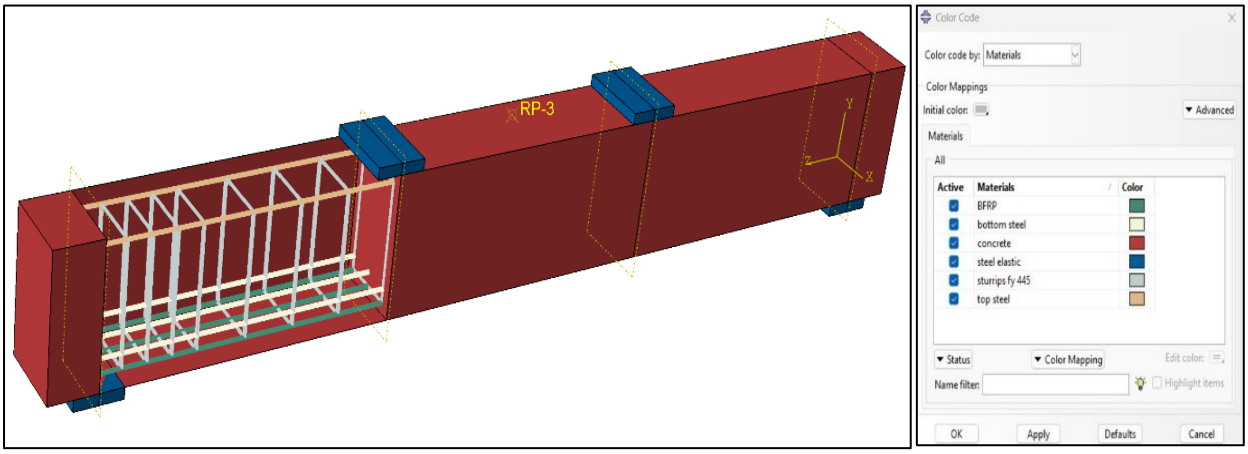

Figure 2. Three-dimensional finite element model of the hybrid reinforced concrete beam showing concrete body, reinforcement, loading and support plates

The modeling strategy employed in this study was based on the following key assumptions:

- Perfect bond between reinforcement and concrete (no bond-slip), which is reasonable for well-confined sections without significant bond deterioration **(Al-Shaarbaf et al., 2017; Abdulrahman, 2025)**.
- Concrete behavior governed by the Concrete Damage Plasticity (CDP) model **(Abaqus Documentation)**.
- Steel reinforcement modeled as elastic-perfect plastic and steel hardening behavior with von Mises yield criterion.
- BFRP reinforcement modeled as a linear elastic material up to rupture.
- Small deformation theory applicable (geometric nonlinearity not considered).
- Quasi-static loading conditions (inertia effects neglected).

3.2 Concrete Modeling

Concrete beam was represented using eight-node three-dimensional hexahedral elements featuring reduced integration (C3D8R). To replicate the nonlinear response of high-strength concrete subjected to combined compression-tension stress states, the Concrete Damage

Plasticity (CDP) model available in ABAQUS was utilized. This CDP model is a continuum-based, plasticity-driven damage framework that incorporates the two primary failure mechanisms observed in concrete: tensile cracking and compressive crushing. It employs principles of isotropic damaged elasticity alongside isotropic tensile and compressive plasticity to depict the inelastic characteristics of concrete. Furthermore, this model takes into account the degradation of material stiffness and the phenomenon of stiffness recovery under cyclic loading in both tension and compression by introducing damage variables, namely d_t(tensile damage) and d_c(compressive damage) **(Flayyih et al., 2020)**.

3.2.1 Plasticity Parameters

The CDP model requires the specification of five plasticity parameters that control the shape of the yield surface and the flow rule. The selection of these parameters significantly influences the predicted structural response, and their values must be carefully chosen based on the concrete type and validated against experimental data. The CDP parameters adopted in this study are presented in **Table 4.**

Table 4. Concrete damage plasticity parameters

$\boldsymbol{\Psi}$	$\boldsymbol{\varepsilon}$	$\boldsymbol{\sigma_{b0}/\sigma_{c0}}$	$\boldsymbol{K_c}$	$\boldsymbol{\mu}$
40	0.1	1.16	0.667	0.0005

Where Ψ is the dilation angle, which controls the volumetric expansion (dilatancy) of concrete for high-strength concrete; dilation angles in the range of 30°-42° have been reported in the literature **(Abdulrahman, 2025; Assi, 2025; Yan and Wang, 2025)**; ε is the eccentricity; σ_{b0}/σ_{c0} denotes the ratio of the initial equiaxial compressive yield stress to the initial uniaxial compressive yield stress; K_c signifies the ratio of the second stress invariant along the tensile meridian; μ is the viscosity parameter.

3.2.2 Compressive Behavior

The empirical model proposed by Lu and Zhao was utilized to characterize the uniaxial compressive stress–strain behavior of high-strength concrete **(Lu and Zhao, 2010)**. **Fig. 3** present the stress–strain relationship in this study that was implemented in ABAQUS using the (CDP) model through the definition of inelastic strain.

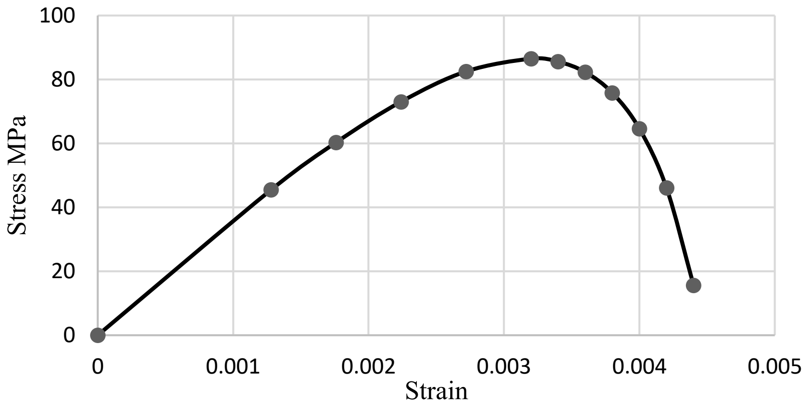

Figure 3. Compressive stress-strain relationship for high-strength concrete used in the CDP model.

The compressive damage parameter (dc) was defined as a function of inelastic strain to represent the degradation of elastic stiffness due to compressive crushing. The compressive damage parameter was calculated using the relationship **(Yu et al., 2010)**.

$$dc = 1 - \frac{\sigma_c}{\sigma_{cu}} \quad (1)$$

Where σ_c is the current compressive stress; and σ_{cu} is ultimate compressive stress.

3.2.3 Tensile Behavior

The tensile behavior of concrete was modeled using a displacement-based softening approach proposed by **(Hordij, 1991)**. This approach improves numerical stability, reduces mesh dependency, and provides a realistic simulation of concrete cracking and energy dissipation. **Fig. 4** showing stress-crack opening displacement curve.

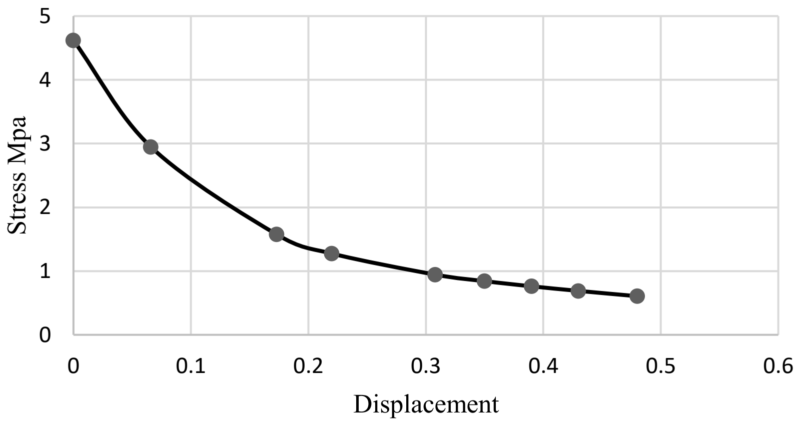

Figure 4. Tensile stress-displacement relationship

The tensile damage parameter (dt) was defined to represent stiffness degradation due to tensile cracking, was calculated using the relationship **(Yu et al., 2010).**

$$dt = 1 - \frac{\sigma_t}{\sigma_{tu}} \quad (2)$$

Where σ_t is the current tensile stress; and σ_{tu} is ultimate tensile stress.

3.3 Steel Reinforcement Modeling

The steel reinforcement bars were modeled using two-node linear three-dimensional truss elements (T3D2). The transverse reinforcement (stirrups 10 mm) and the top longitudinal bars (6mm) were defined as elastic–perfectly plastic. This assumption is considered adequate since these reinforcement components typically do not experience significant cyclic plastic strain demands and mainly contribute to confinement and crack control, rather than governing the flexural response. In contrast, the bottom longitudinal reinforcement (10mm) was modeled incorporating strain hardening behavior presented by **(Yun and Gardner, 2017)**. This approach was adopted to more realistically capture the cyclic response of the beam, as the bottom reinforcement is the primary load-carrying component under flexure and is subjected to repeated tensile loading. Including strain hardening allows for a more accurate representation of stiffness degradation, energy dissipation, and the evolution of flexural capacity under repeated loading. **Table 5** presents material properties for steel-reinforced bars.

Table 5. Material properties for steel-reinforced bars

Bar diameter (mm)	Elastic properties		Elastic–perfectly plastic		Strain hardening behavior
	E (GPa)	υ	σ_{yield}	ε_{in}^{pl}	
6	200	0.3	402	0	/
10	200	0.3	445	0	**Fig. 5** shows strain hardening behavior for bottom steel reinforcement only.

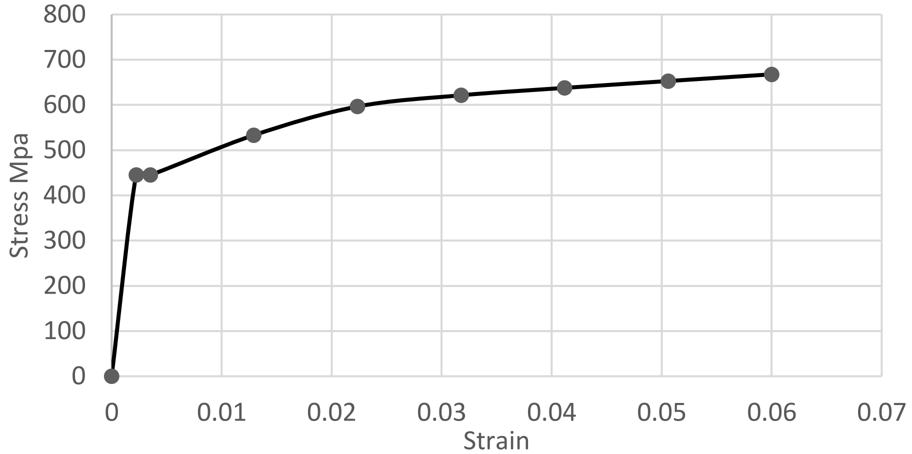

Figure 5. Strain hardening behavior for bottom steel reinforcement

3.4 BFRP Reinforcement Modeling

The BFRP reinforcement bars were also modeled using two-node linear three-dimensional truss elements (T3D2), identical to the element type used for steel reinforcement. However, the material constitutive model for BFRP differed significantly from steel due to the brittle, linear elastic nature of fiber-reinforced polymer composites. The elastic and plastic model was employed to characterize the mechanical properties of the BFRP bars, as detailed in **Table 6**.

Table 6. The input ABAQUS parameters of BFRP bar

Bar diameter (mm)	Elastic properties		Plastic properties	
	E (GPa)	υ	σ_{yield}	ε_{in}^{pl}
10	55	0.28	950	0

3.5 Supporting and Loading Steel Plates Modeling

The steel bearing plates at support and loading locations (150 mm x 50 mm x 50 mm) were also modeled using C3D8R elements. These plates were assigned linear elastic material properties with high stiffness (Es=200 GPa) and (υ=0.3) to represent the rigid steel plates used in the experimental setup and to prevent stress concentrations and local crushing of concrete at load application and support points. To prevent local stress concentrations and numerical instabilities at the contact points, the steel bearing plates were tied to the concrete surface using a Tie constraint, ensuring compatible deformation at the interface.

3.6 Boundary Conditions and Loading

The (displacement / rotation) boundary conditions were defined to replicate the simply supported configuration used in the experimental setup (Pin and Roller):

- ***Left support (pin)***: All translational degrees of freedom were restrained (U1=U2=U3=0) at the nodes on the bottom surface of the left bearing plate, while rotations were left free.
- ***Right support (roller)***: The out-of-plane translational degree of freedom (U1=0) and the vertical translational degree of freedom (U2 = 0) were restrained at the nodes on the bottom surface of the right bearing plate, while the longitudinal translation (U1) and all rotations were left free.

The loading was applied through steel loading plates positioned at the two loading points. A reference point (RP3) was defined at the midspan of the beam, representing the location of load application. The reference point was coupled to the plates by coupling constraint, so the load would be transferred to the beam through the plates.

A Static General analysis was used to definition the load in ABAQUS. The beams were subjected to a two-step loading protocol. The first step represented repeated loading, which was applied as a concentrated force at RP3 using an amplitude definition to simulate loading-unloading cycles to a specified number of cycles. Figure 6 shows the amplitude and repeated load definition. Upon completion of the repeated step, the second stage (monotonic loading) begins, in which displacement-controlled loading was applied at RP3 and continued until failure to ensure accurate representation of the post-peak response and structural behavior until failure.

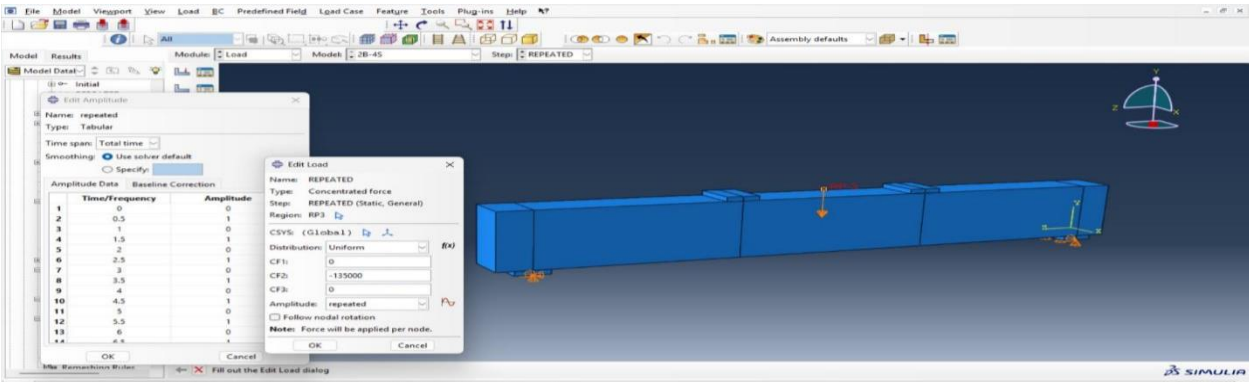

Figure 6. The amplitude and repeated load definition

3.7 Interaction Modeling

3.7.1 Interaction between Concrete and Reinforcement

The interaction between reinforcement and concrete was modeled using the Embedded Region constraint, which enforces perfect bond between the reinforcement (embedded elements) and the surrounding concrete (host elements). **Fig. 7** shows the interaction between concrete and reinforcement.

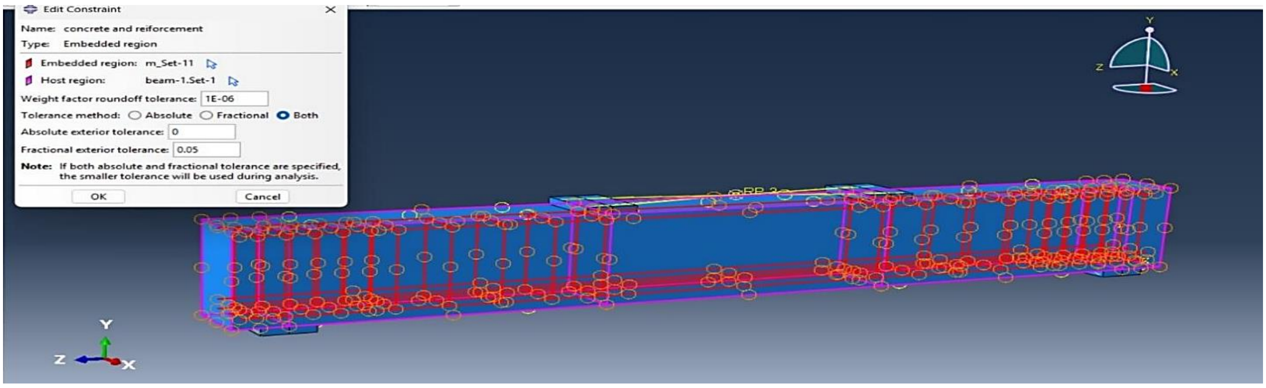

Figure 7. The interaction between concrete and reinforcement in ABAQUS

3.7.2 Interaction between Concrete and Plates (Loading and Supports)

The interaction between the concrete surface and the steel plates was defined using a tie constraint. This approach assumes a perfect bond between the two surfaces, preventing any relative displacement or separation at the interface.

3.8 Meshing of Element

The process of meshing means to divide the model into smaller elements. The accuracy and reliability of the numerical results depended upon the mesh size. To ensure the convergence of the numerical results between accuracy and computational efficiency, mesh convergence analysis was performed on the beam model 2B-4S. Four different mesh sizes were considered for the beam model: 30 mm, 25 mm, 20 mm, and 15 mm, corresponding to approximately 2640, 4800, 10400, and 22780 elements, respectively, as shown in **Fig. 8.**

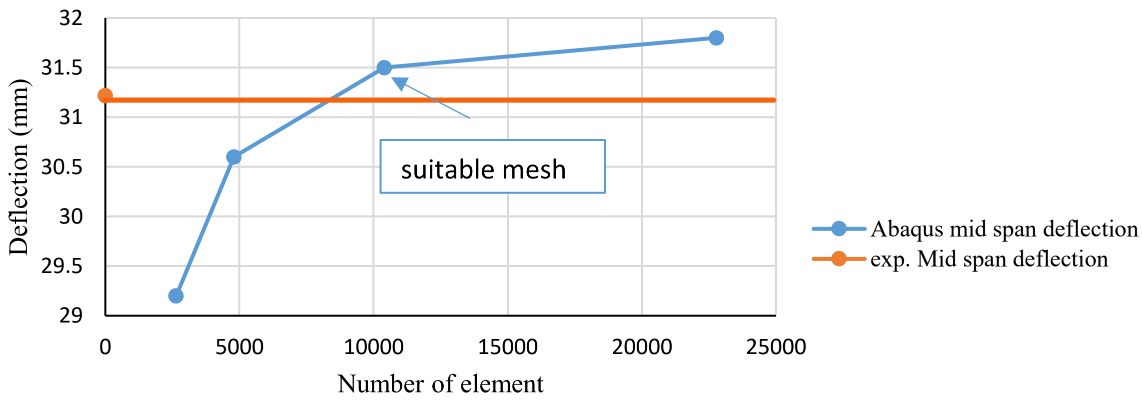

Figure 8. The relation of the number of elements and deflection

Mesh sensitivity results show that decreasing the element size from 30 mm to 20 mm has a significant effect on the response of the structure, especially on the midspan deflection, which matches the experimental values. Further refinement from 20 mm to 15 mm increases the deflection by only a slight amount, suggesting that we are close to convergence and further refinement does not significantly improve the result. Therefore, a mesh size of 20 mm was adopted for the concrete element in the final model. The reinforcement bars (both steel and BFRP) and the steel bearing plates were meshed with a similar element size of 20 mm. **Fig. 9** shows a 20 mm element size for concrete and reinforcement.

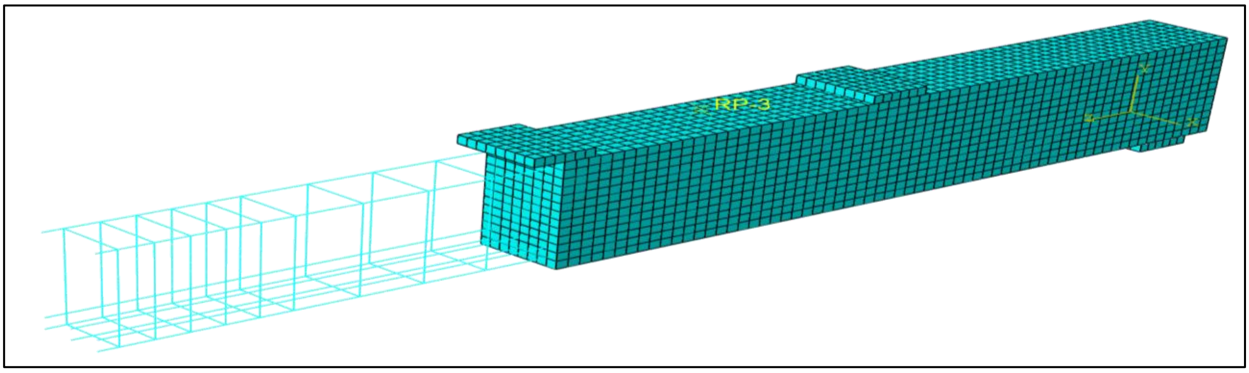

Figure 9. Finite element mesh of the hybrid reinforced concrete beam showing 20 mm element size for all parts element

4. VALIDATION OF THE NUMERICAL MODEL

4.1 Load-Deflection Relationship

The validity of the developed finite element model was assessed by comparing the numerical predictions with experimental results for all beams. The experimental data utilized for the validation of the proposed 3D finite element model was adopted from a comprehensive experimental study conducted by **(Kadhim and Hassan, 2026)**. The primary validation metric was the load-deflection behavior, which captures the overall structural behavior. The load-deflection curve and vertical numerical deflection for the examined beams are shown in **Figs. 10 to 15.**

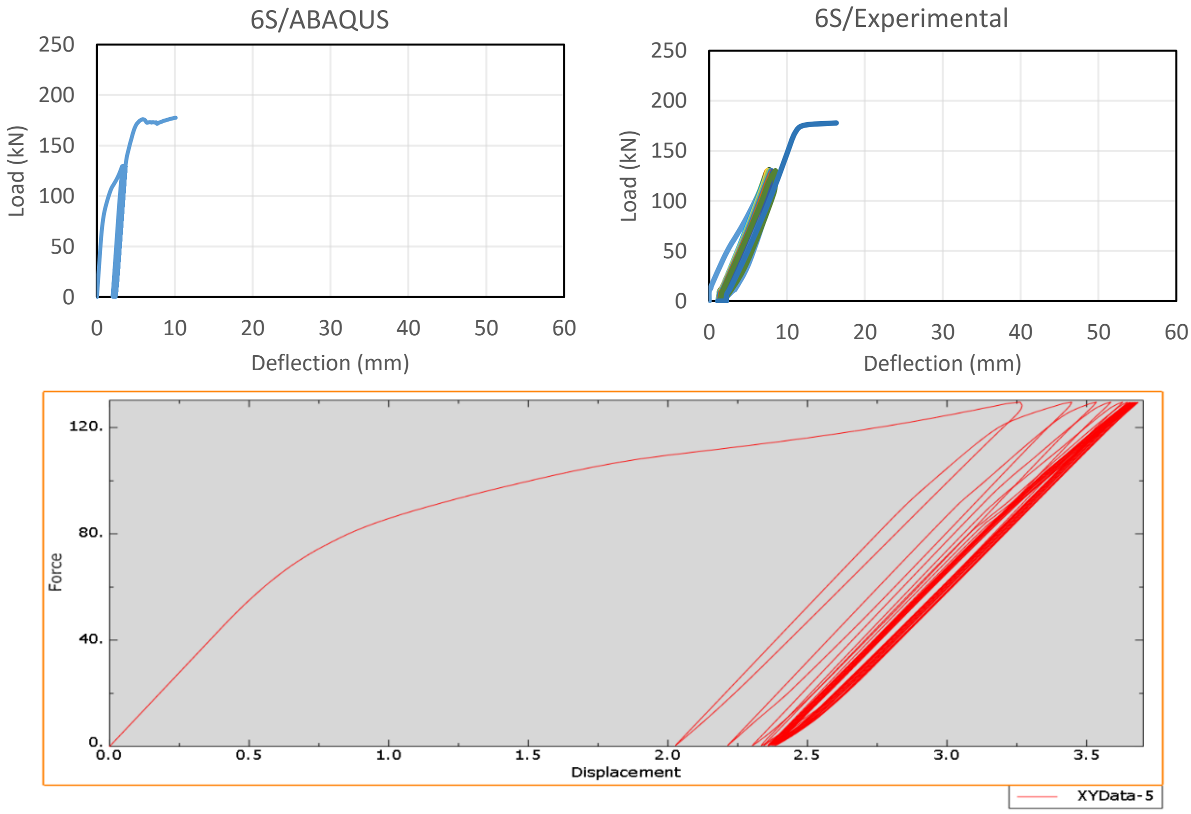

Figure 10. (a) Experimental and Numerical load-deflection curves for beam 6S
(b) Illustration of the repeated loading stage in ABAQUS for Beam 6S

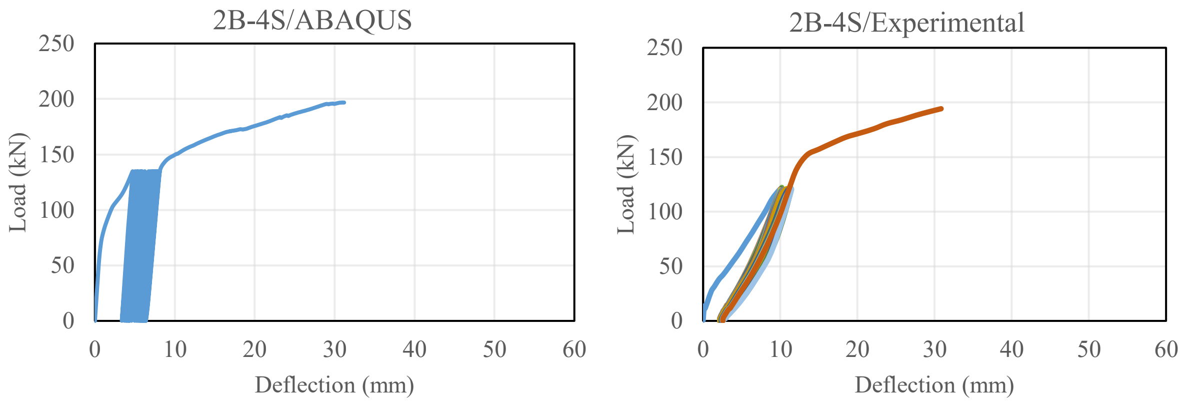

Figure 11. Experimental and Numerical load-deflection curves for beam 2B-4S

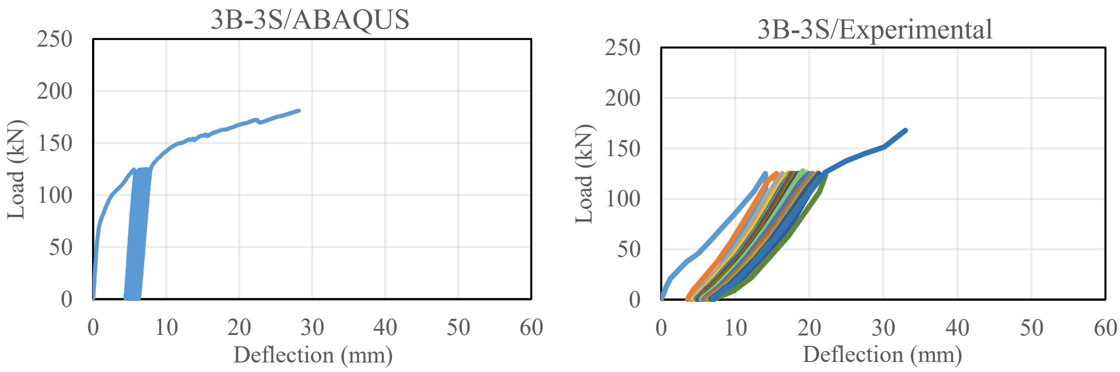

Figure 12. Experimental and Numerical load-deflection curves for beam 3B-3S

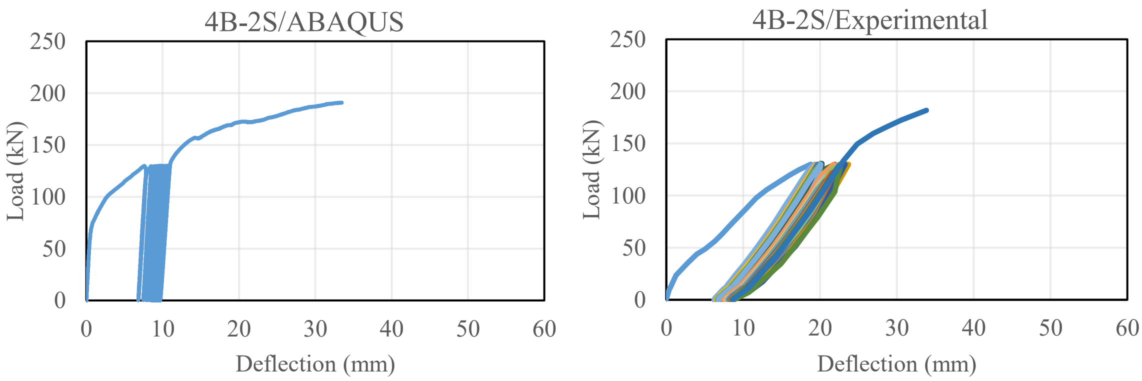

Figure 13. Experimental and Numerical load-deflection curves for beam 4B-2S

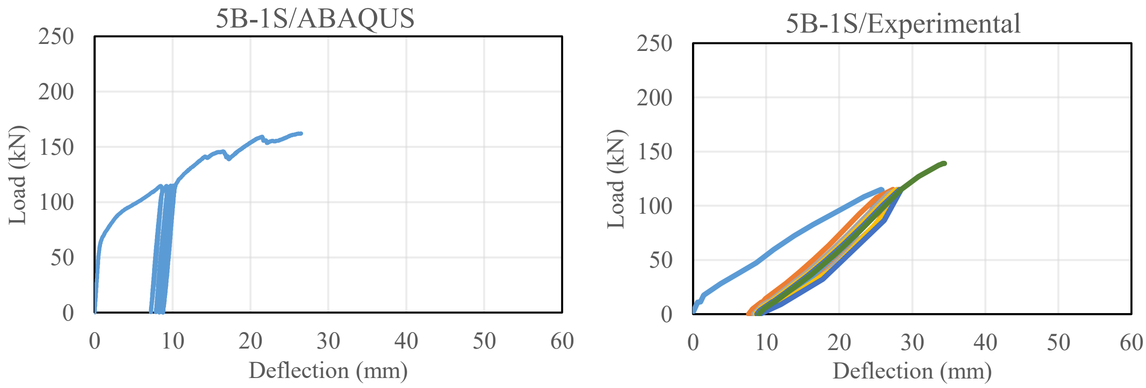

Figure 14. Experimental and Numerical load-deflection curves for beam 5B-1S

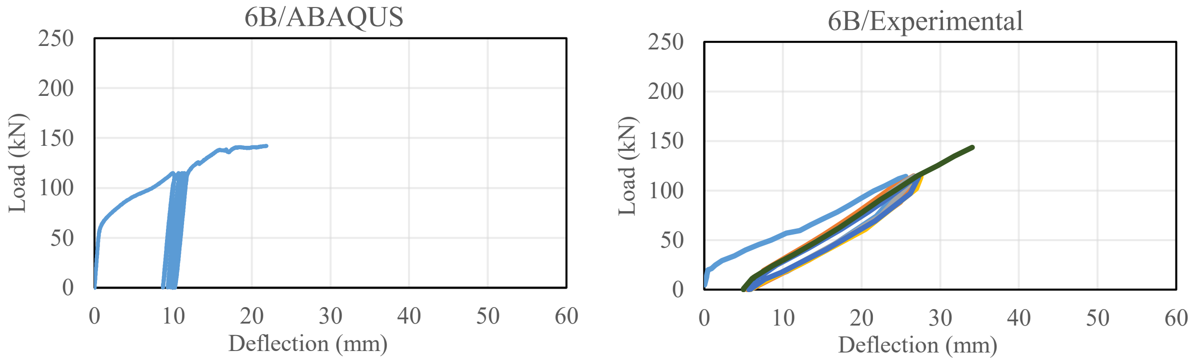

Figure 15. Experimental and Numerical load-deflection curves for beam 6B

The validation focused on comparing the ultimate load capacity and maximum mid-span deflection obtained from the monotonic loading stage following the repeated loading, which is explained in Table 7. The numerical model demonstrated excellent accuracy in predicting ultimate load capacity, with errors ranging from 0.16% (beam 6S) to 11.15% (beam 3B-3S), and an average absolute error of approximately 5% across all six beams. This level of accuracy is well within the acceptable range reported in similar studies of reinforced concrete beams using finite element analysis. **(Al-Shaarbaf et al., 2017)** reported that their FE model accurately predicted experimental response with similar error magnitudes, and **(Yan and Wang, 2025)** reported ultimate capacity errors within 10% for FRP-concrete hybrid beams, which they considered satisfactory validation.

However, the deflection predictions exhibited greater variability, with errors ranging from 0.12% (beam 2B-4S) to 36.31% (beam 6B), and an average absolute error of 17 %. The finite element model consistently underestimates the deflection. This underestimation becomes more pronounced in beams subjected to fewer loading cycles, such as the two beams with the highest deflection errors 5B-1S (25.9%) and 6B (36.31%), which are both BFRP-dominant beams with high BFRP reinforcement ratios and minimal or no steel reinforcement. In contrast, the hybrid beams with more balanced steel-to-BFRP ratios (2B-4S, 3B-3S, 4B-2S) exhibited excellent deflection agreement, with errors of 0.12%, 11.71%, and 1.15%, respectively. This behavior may be attributed to the inability of the numerical model to accurately capture the stiffness degradation and damage accumulation under repeated loading, particularly when the cyclic history is limited.

Table 7. Comparison of Experimental and Numerical Results

Beam ID	Maximum repeated load (kN)	No. of cycle	Experimental Result		Numerical Result		Absolute difference Load (%)	Absolute difference Deflection (%)
			Ultimate static load (kN)	Maximum deflection (mm)	Ultimate static load (kN)	Maximum deflection (mm)		
6S	130	24	177.8	14.33	177.5	10.12	0.16	29.3
2B-4S	135	25	194.3	31.22	196.79	31.18	1.28	0.12
3B-3S	125	24	162.8	32.27	180.96	28.49	11.15	11.71
4B-2S	130	24	181.7	33.84	190.74	33.45	4.97	1.15
5B-1S	115	5	146.4	35.8	162	26.5	10.65	25.9
6B	115	5	144.4	34.31	142.05	21.85	1.62	36.31
Average absolute difference	/	/	/	/	/	/	4.97	17.44

The apparent discrepancy in deflection between BFRP-dominated specimens (36.31% for beam 6B) is due to the difficulties with modeling the damage accumulation under repeated loading of non-ductile reinforcements. The CDP model tends to provide a stiffer response, which is commonly observed in RC modeling due to the assumption that the bond is perfect and that the material homogeneity is idealized.

Unlike the experiment results, the numerical curve of load-deflection of all beams is stiffer than the real curve. There are some possible differences between the experimental and numerical results, which can be explained by the following:

1. Idealized material behavior: The FE model assumes that the concrete has homogenous material properties, but in actuality there are micro-cracks, voids and heterogeneities that affect deformation and stiffness. The presence of such microscopic nonlinearities, like aggregate interlocking and localized tension stiffening, explains why the numerical response is stiffer on the unloading-reloading paths.
2. Perfect bond assumption: The FE model utilized the 'Embedded Region' constraint, which assumes a perfect bond between the reinforcement and concrete. In reality, repeated loading causes micro-slips and localized bond degradation at the steel-concrete and BFRP-concrete interfaces, leading to greater experimental deflections.
3. Boundary condition idealization: The numerical model assumes perfect Pin – roller support, while experimental setups may include friction and minor restraint which affect deformation behavior.
4. Simplified cyclic damage representation: Although the CDP model accounts for stiffness degradation, it does not fully capture cumulative damage effects under repeated loading. Particularly for beams subjected to a limited number of cycles. Cumulative micro-damage in the concrete matrix under repeated cycles can reduce the effective modulus of elasticity, a phenomenon that is challenging to capture perfectly with monotonic-based damage parameters. The repeated loading in the numerical model has sharp unloading-reloading paths, unlike the smoother response of the experimental model due to the real material nonlinearities and energy dissipation.

These factors led to an increase in the stiffness of the beam subjected to repeated loading, which is reflected in the downward trend of the unloading condition is identical to the slope of the line for the elasticity stage. This causes high residual deflection. Such behavior is in good agreement with the findings reported by **(Flayyih et al., 2020)**, who observed similar high stiffness and residual deformation characteristics under repeated loading.

The apparent yield-like point observed in the first loading cycle and monotonic stage for beams (5B-1S and 6B) does not represent actual yielding of the BFRP reinforcement, as FRP materials exhibit a linear elastic response up to rupture without a distinct yield stage. Instead, this point corresponds to the transition from the uncracked to cracked state of the concrete, accompanied by stiffness degradation due to crack initiation and propagation. A similar feature can also be identified in the experimental response, but it occurs at relatively low load levels and is therefore less apparent at first glance. In contrast, this transition becomes more pronounced in numerical results due to the higher stiffness predicted by the finite element model, giving the impression of a yield-like point.

Moreover, a comparable behavior can be observed from the load–deflection response presented by **(Flayyih et al., 2020)** for beam C7%-HGC-2. Although not explicitly discussed by the authors, the curve exhibits a noticeable change in stiffness at an early stage of loading, which is consistent with the apparent yield-like point identified in the present study. This further supports the theory that this transition in stiffness may result in cracking and deterioration rather than yielding of the reinforcement.

Furthermore, the localized oscillations in the numerical load-deflection curve indicate the complex numerical convergence at the onset of severe concrete softening. To address this, viscous regularization was employed; while this ensures solution stability, it may lead to slight deviations from the experimental curve's smoothness. However, the high accuracy of the model in predicting ultimate capacity (averaging ~5% error) and the excellent qualitative agreement in crack patterns **(Figs. 16 to 21**) confirm that the model is sufficiently robust for the subsequent parametric investigation. Despite these discrepancies, the numerical and experimental results agree on most aspects. This confirms the accuracy of the developed finite element model and that the CDP parameters, element types, mesh size, and assumptions are appropriate to simulate the behavior of high-strength concrete beams reinforced with hybrid steel/BFRP.

4.2 Crack Patterns

As well as the response to load-deflection, crack patterns were also checked in the numerical model against the experimental results; these are shown in **Figs. 16 to 21** at the failure stage.

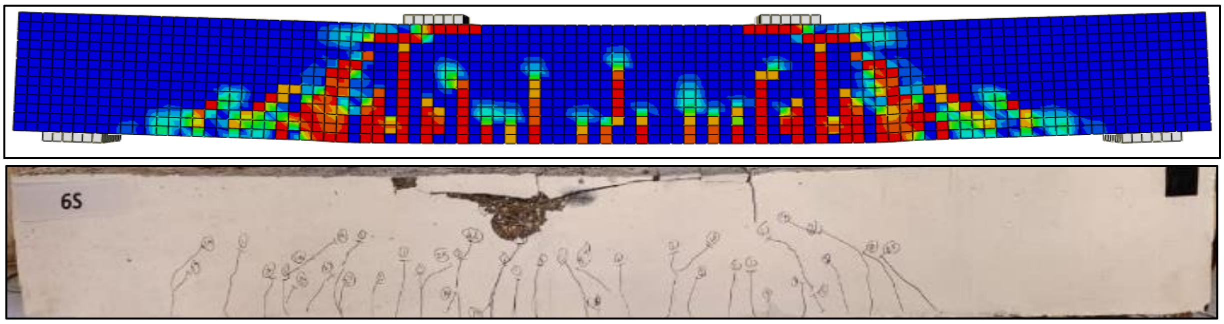

Figure 16. Experimental and Numerical crack distribution for beam 6S

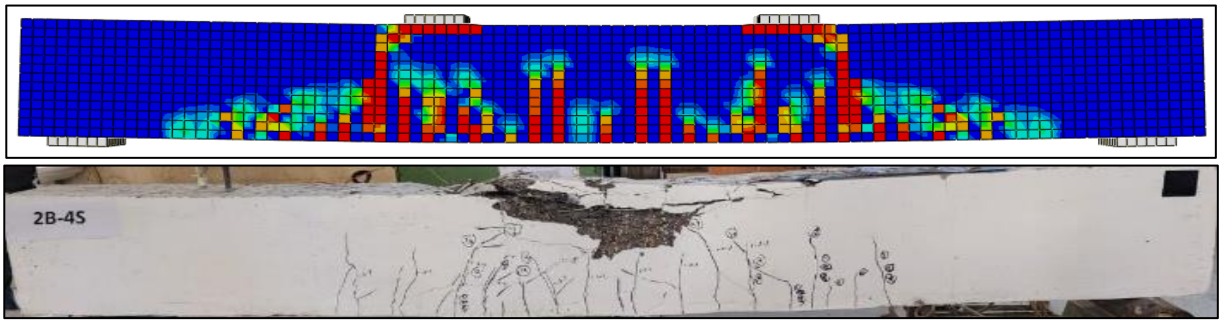

Figure 17. Experimental and Numerical crack distribution for beam 2B-4S

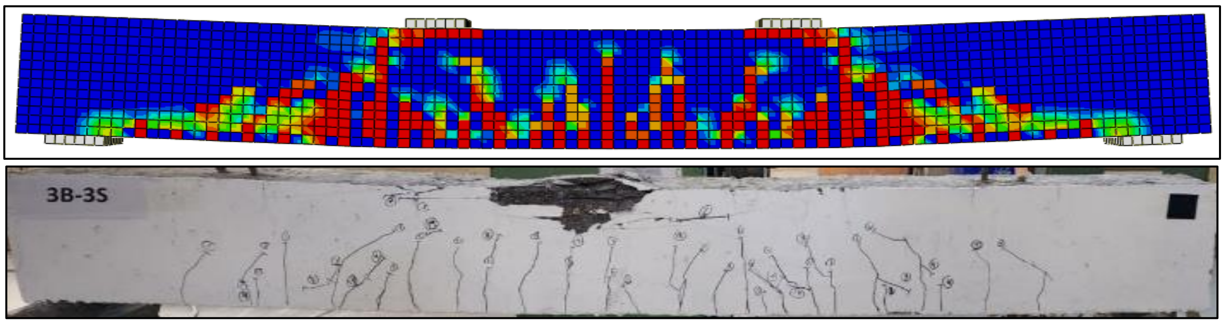

Figure 18. Experimental and Numerical crack distribution for beam 3B-3S

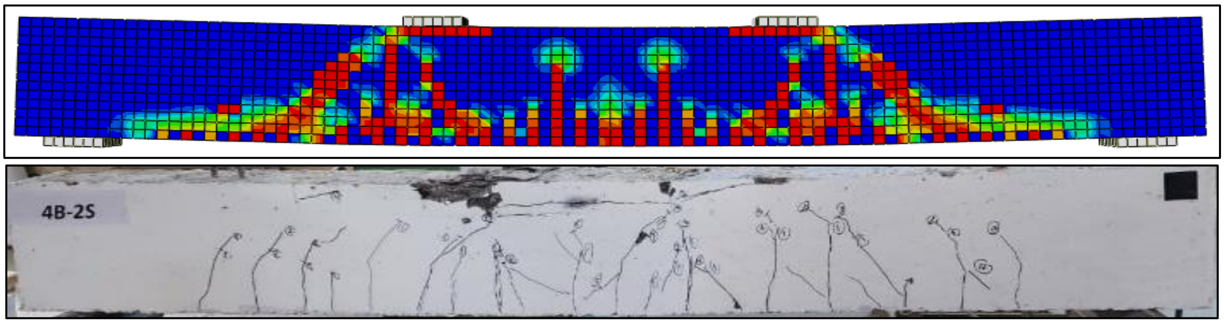

Figure 19. Experimental and Numerical crack distribution for beam 4B-2S

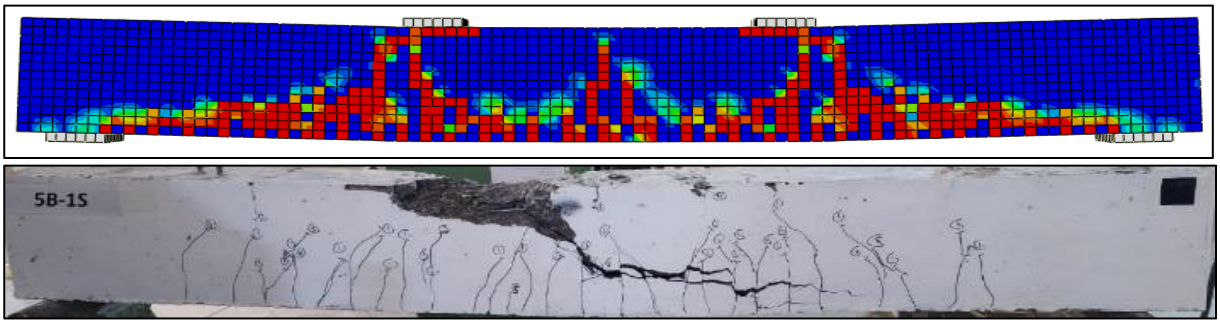

Figure 20. Experimental and Numerical crack distribution for beam 5B-1S

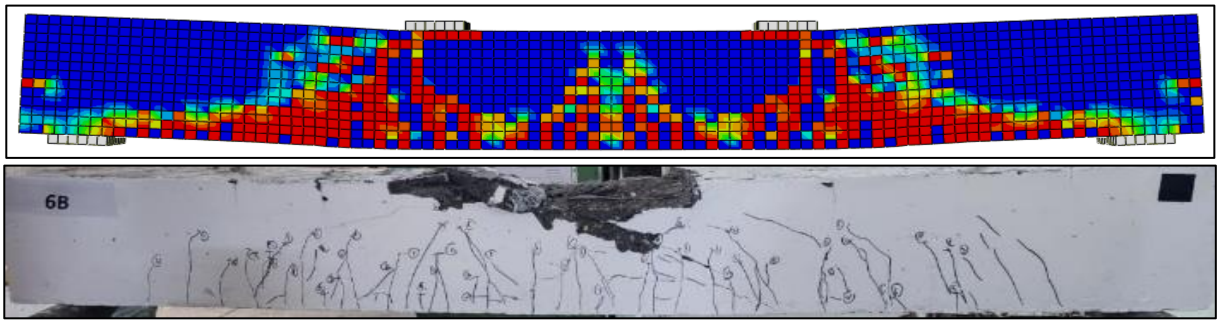

Figure 21. Experimental and Numerical crack distribution for beam 6B

The crack patterns predicted by the finite element model, visualized using the tensile damage variable (DAMAGET) contours in ABAQUS, showed satisfactory correlation with the experimental crack patterns, accurately replicating the location and distribution of flexural cracks in the constant moment region (between the two loading points) at the bottom fiber of the beam, where tensile stresses are maximum. As loading progressed, these flexural cracks propagated vertically toward the neutral axis, and additional cracks formed along the constant moment region. The crack distribution predicted by the model was consistent with experimental observations. The DAMAGET contours also showed damage concentration at the bottom fiber in the constant moment region, representing tensile cracking, and damage concentration at the top fiber near the loading points, representing compressive crushing.

4.3 Distribution of Stresses at Reinforcement Bars

The stresses of the reinforcement are one of the ABAQUS outputs to identify the mode of failure and verify the load transfer mechanism. **Figs. 22 to 27** describe the numerical stress distribution of reinforcement for all beams at ultimate load.

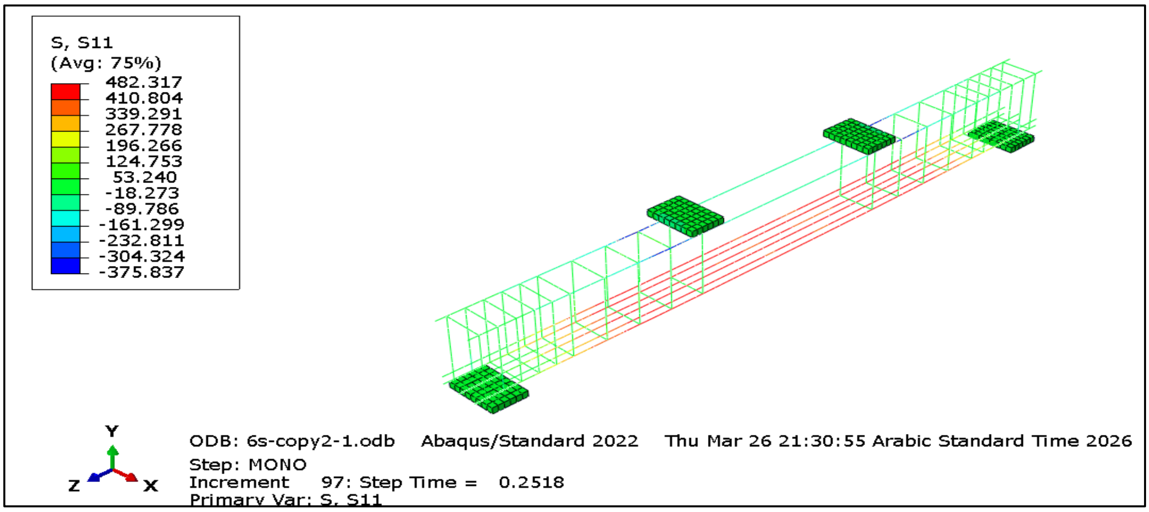

Figure 22. Numerical stresses of reinforcement for beam 6S

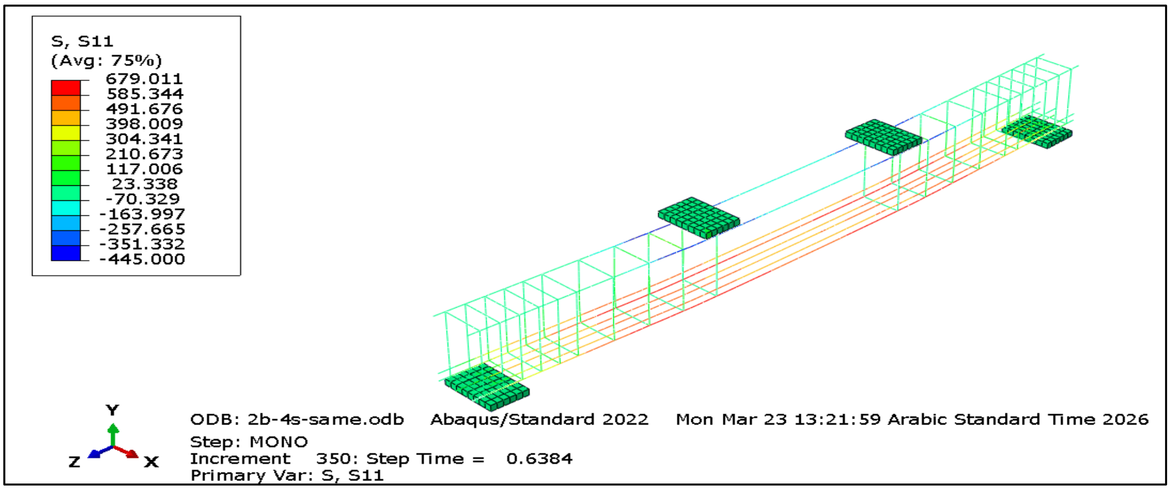

Figure 23. Numerical stresses of reinforcement for beam 2B-4S

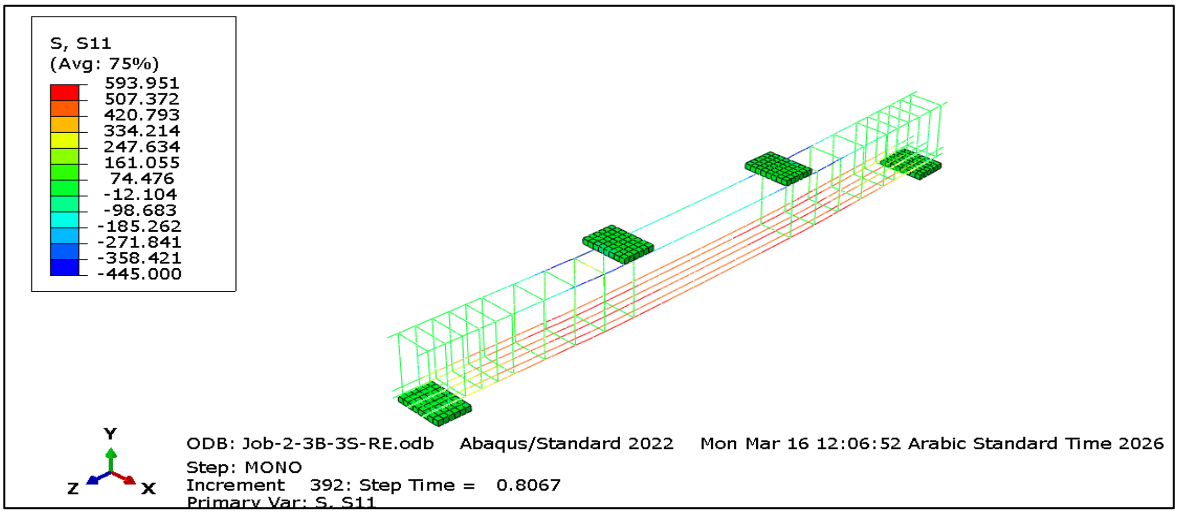

Figure 24. Numerical stresses of reinforcement for beam 3B-3S

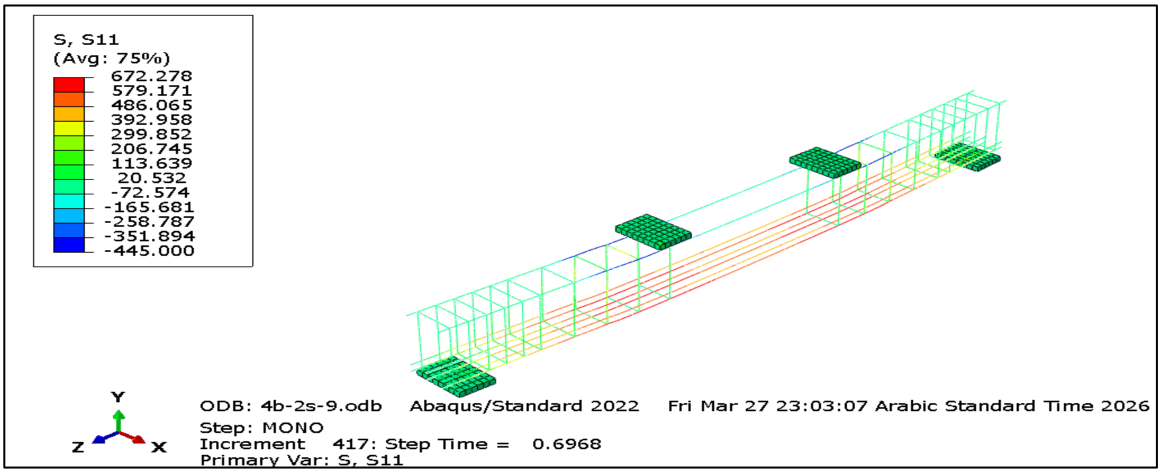

Figure 25. Numerical stresses of reinforcement for beam 4B-2S

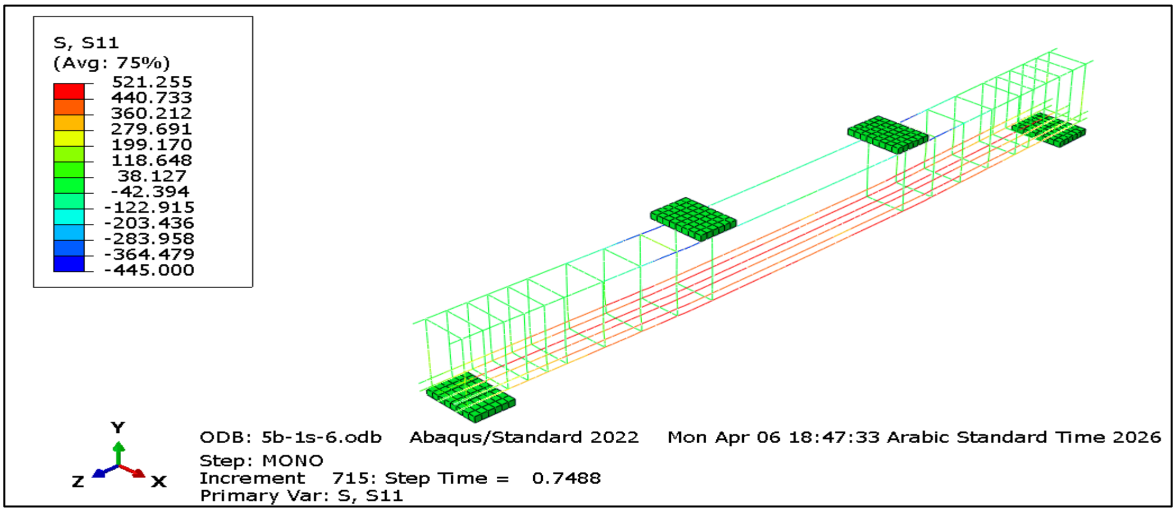

Figure 26. Numerical stresses of reinforcement for beam 5B-1S

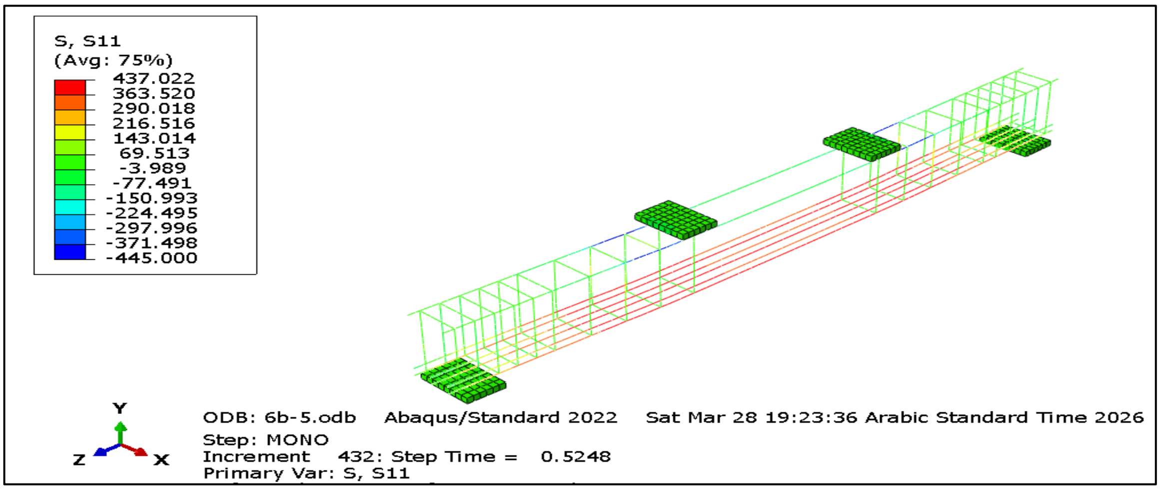

Figure 27. Numerical stresses of reinforcement for beam 6B

The stress distribution in reinforcement bars obtained from the numerical analysis confirmed the expected behavior. In the constant moment region, the stress was relatively uniform, while the stress decreased toward the support. The stress distribution in the reinforcement indicates that the dominant failure mode in all beams was characterized by yielding of the steel reinforcement, followed by subsequent concrete crushing (6B failure was governed only by concrete crushing). Furthermore, the BFRP bars did not reach their ultimate tensile capacity in any specimen, indicating that rupture of BFRP did not control the failure mechanism. Although experimental strain gauges were installed, local measurements became unreliable as the beams approached ultimate capacity due to extensive cracking and high strain gradients. Therefore, global load-deflection behavior is used as the primary validation metric. The high correlation in global response (4.97% error in ultimate load) provides implicit validation of the model's internal mechanical consistency. These outcomes agree with the experimental results and confirm the reliability of the numerical model in capturing the actual failure modes.

5. PARAMETRIC STUDY: THE EFFECT OF CONCRETE COMPRESSIVE STRENGTH

The experimental program and numerical validation revealed the dominant failure mode in all beams was concrete crushing in the compression zone; which occurred before the BFRP bars reached their maximum tensile strength of 950 MPa. The resulting premature failures prevent the effective use of the BFRP's excellent tensile strength, which is one of the major advantages of using this material**. (Al-Zahrani et al., 2023)** noted that BFRP beams often fail through concrete crushing, and that by strengthening the concrete, more of the FRP tension can be captured, increasing the overall structural capacity. **(Salem and Issa, 2023)** confirmed via a validated nonlinear finite element analysis that increasing the concrete strength affects the mode of failure and FRP stress development, although the magnitude of this gain depends on geometry, reinforcement ratio, and assumptions.
The parametric study focused on hybrid reinforcement beams (with high no. of cycles) (2B-4S, 3B-3S and 4B-2S) Which, demonstrated a high level of accuracy when compared with the experimental data. To investigate the potential for improving BFRP utilization and structural performance, a parametric study was conducted by increasing the concrete compressive strength to 120 MPa. While all reinforcement properties (steel and BFRP), beam geometry, boundary conditions, and loading procedures remained identical to the reference model. Initially, the beams were subjected to monotonic loading up to failure to determine their ultimate load. Subsequently, 70% of the obtained ultimate load was adopted as the peak amplitude for the repeated loading stage. Thereafter, the same loading protocol used for the reference beams was applied, consisting of repeated loading followed by a final monotonic loading stage up to failure.

5.1 Effect on Ultimate Load Capacity

The parametric study results for ultimate load capacity are presented in **Table 8,** which compares the ultimate load predicted by the finite element model for different concrete strengths. The results show that increasing the concrete compressive strength from 86.5 MPa to 120 Mpa increases the ultimate load capacity for all beam configurations, with a varying degree of increase depending on the type and ratio of reinforcement. The results demonstrate that the percentage increase in ultimate load capacity is strongly correlated with the BFRP reinforcement ratio. For the hybrid beams with the highest steel content (2B-4S), ultimate load capacity increased by 27.93%, since steel yielding still prevails, but the increased compression zone capacity allows for slightly higher post-yield loads. By contrast, the hybrid beams with the highest BFRP content (3B-3S and 4B-2S) showed more significant increases in ultimate capacity (48.58% and 43.28%, respectively).

Table 8. Effect of Concrete Strength on Ultimate Load Capacity

Beam ID	Ultimate Load at $f'c$ = 86.5 Mpa (kN)	Ultimate Load at $f'c$ = 120 Mpa (kN)	Increase (kN)	Increase (%)
2B-4S	196.79	251.76	54.97	27.93
3B-3S	180.96	268.69	87.73	48.48
4B-2S	190.74	273.31	82.57	43.28

This trend indicates that the structural performance of hybrid beams is governed by the balance between tensile reinforcement capacity and compression Zone capacity. When concrete strength is low, the compression zone limits the contribution of BFRP. Increasing concrete strength shifts this balance, allowing greater mobilization of BFRP tensile capacity. The mechanism behind the tensile and compressive capacity increases is as follows: In a reinforced concrete beam that is bent, the ultimate moment is determined by the balance of the tensile force in the reinforcement and the compressive force in the concrete compression zone. For BFRP reinforcement, the tensile force is limited by the rupture of BFRP ($Tf = Af \times fu = Af \times 950$ Mpa) or by concrete crushing in the compression zone. Because the strength of the concrete is 86.5 Mpa, the compression zone capacity of the concrete is not strong enough to compensate for the full tensile strain of BFRP bars and thus the concrete will be crushed prematurely. By increasing the concrete strength to 120 Mpa, the compression zone can sustain higher compressive stress and forces, and the neutral axis is lifted up and the BFRP bars develop higher tensile strains and stresses before the concrete becomes fully crushed. This can be particularly useful with beams with high BFRP content, because the potential tensile force is high, but the compression zone is the limiting factor.

5.2 Effect on BFRP Stress and Failure Mode

One of the most significant results of parametric study is the influence of concrete strength on BFRP stress. **Table 9** shows the maximum tensile stress in the BFRP bars at ultimate load for both concrete strengths, along with BFRP Stress Utilization Ratio (U_f), which is defined as the ratio of the maximum tensile stress developed in the BFRP bars at the ultimate load (f_f) to their ultimate tensile strength (f_{fu}), (f_f / f_{fu})*100), and failure mode.

Table 9. Effect of Concrete Strength on BFRP Stress Utilization

Beam ID	(f_f) at $f'c$ = 86.5 MPa (kN)	(U_f) at 86.5 Mpa (%)	(f_f) at $f'c$ = 120 Mpa (kN)	(U_f) at 120 Mpa (%)	The increase in U_f (%)	Failure Mode at 86.5 Mpa	Failure Mode at 120 Mpa
2B-4S	679	71.47	938	98.73	38.14	Steel yield + CC*	BFRP rupture
3B-3S	594	62.52	940	98.94	58.24	Steel yield + CC	BFRP rupture
4B-2S	672	70.73	914	96.21	36	Steel yield + CC	BFRP rupture

*CC = Concrete crushing

Results show that increasing concrete strength enhances the BFRP stress utilization for all hybrid beams. For the reference concrete (86.5 Mpa), the BFRP Stress Utilization Ratio indicate that 62–72% of the BFRP tensile capacity was utilized before the concrete crushed.

This implies an underutilization of the BFRP material and a failure to fully use its best feature (high tensile strength).

When the concrete strength was increased to 120 Mpa, the BFRP utilization ratios increased dramatically. Beam 3B-3S exhibited the highest improvement in BFRP utilization (58.24%), with final utilization ratios of 98.94. At the lower concrete strength (86.5 Mpa), this beam did not fully benefit from either reinforcement component; the steel ratio was insufficient to develop high load-carrying capacity, while the BFRP ratio was also not dominant enough to mobilize its full tensile strength. Consequently, the beam showed limited performance. However, increasing the concrete strength enhanced the compression zone capacity, allowing both steel and BFRP to be more effectively engaged, resulting in the highest gain in utilization among all beams. Beam 4B-2S, which contains a higher proportion of BFRP, showed a significant increase in load capacity due to the dominant contribution of the BFRP reinforcement. Nevertheless, despite the high stress levels developed in the BFRP bars (913 Mpa), the ultimate tensile strength was not reached at the ultimate load. For beam 2B-4S, which has the lowest BFRP ratio, the BFRP bars achieved near-full utilization under higher concrete strength. However, the overall behavior remained governed by the steel reinforcement and the compression zone.

Importantly, the numerical results indicate that for beams (2B-4S and 3B-3S), the maximum BFRP stress at ultimate load remained slightly below the rupture strength (950 Mpa). This confirms that BFRP rupture did not occur at the peak load. However, beyond the peak load, as the load decreased and deflections continued to increase, the BFRP stresses continued to rise, eventually reaching the rupture limit. This behavior suggests that the failure at ultimate load was not induced by BFRP rupture but was a consequence of other factors, such as concrete crushing or yielding.

Thus, based on this observation, it is possible that further increasing the concrete compressive strength beyond 120 Mpa will be insufficient to use the full tensile power of the BFRP, especially for beams with higher BFRP ratios, such as 4B-2S. However, from a design perspective, allowing BFRP rupture is not desirable, as it leads to a brittle and sudden failure mode. Therefore, design guidelines typically limit the effective stress in BFRP using reduction or environmental factors to prevent reaching the ultimate tensile strength **(ACI Committee 440, 2015; ACI Committee 440, 2022; Tran et al., 2025)**.

Overall, increasing concrete strength allows the compression zone to sustain higher compressive stresses at the same strain level, which shifts the neutral axis upward (reduces c). This upward shift of the neutral axis increases the distance from the neutral axis to the reinforcement level (d – c), which in turn increases the tensile strain in the reinforcement for a given top fiber compressive strain. Consequently, the BFRP bars can develop higher tensile strains and stresses before the concrete reaches its ultimate compressive strain, enhancing the efficiency of BFRP utilization, but the desirable structural response is achieved when high utilization is attained without reaching rupture, ensuring a more controlled and safer failure mechanism.

5.3 Effect on Load-Deflection Behavior

The effect of concrete strength on load-deflection behavior was analyzed by comparing the load-deflection curves predicted by the finite element model for concrete strengths of 86.5 MPa and 120 Mpa (shown in **Figs. 28 to 30**).

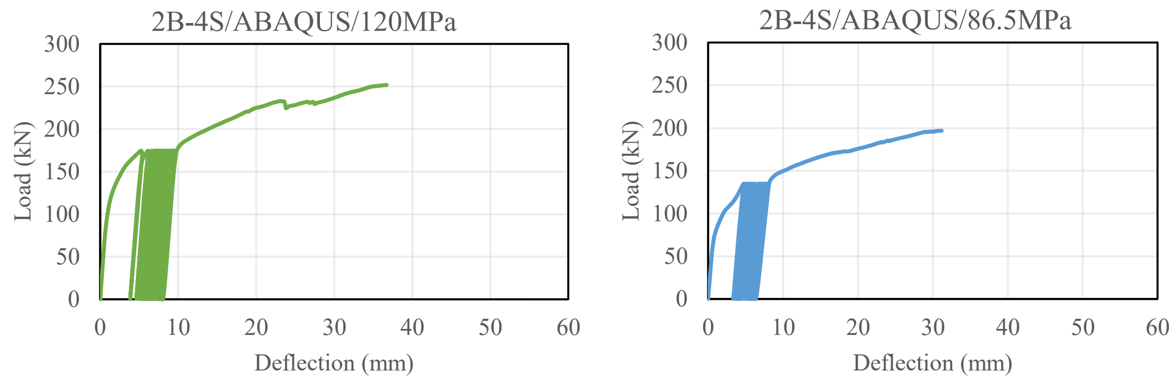

Figure 28. Numerical load-deflection curves for beam 2B-4S for 86.5 and 120 Mpa compressive strength

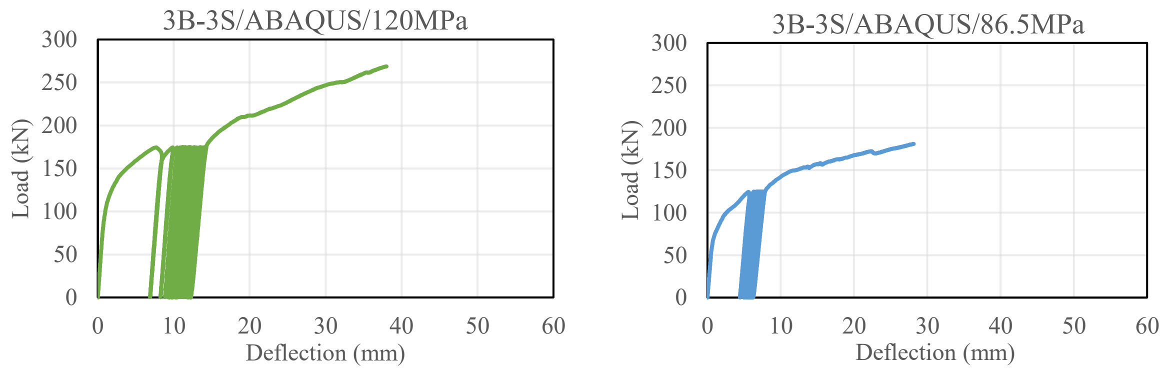

Figure 29: Numerical load-deflection curves for beam 3B-3S for 86.5 and 120 Mpa compressive strength

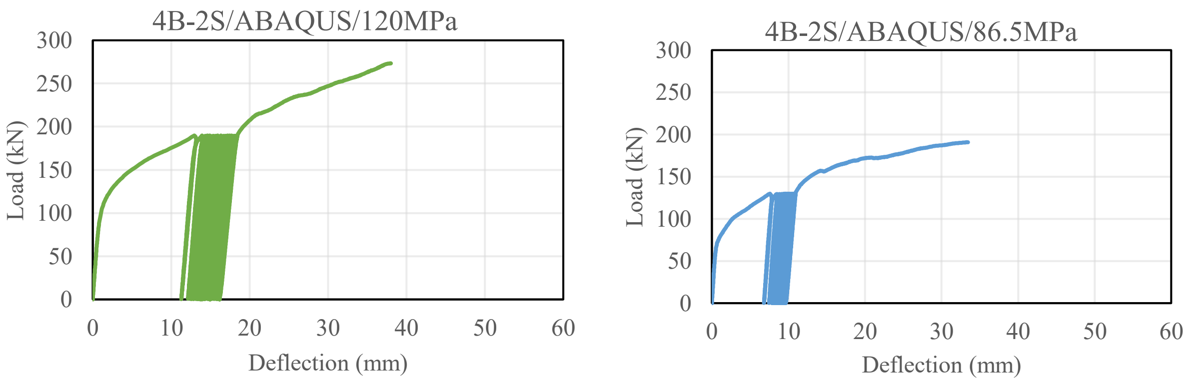

Figure 30. Numerical load-deflection curves for beam 4B-2S for 86.5 and 120 Mpa compressive strength

The load–deflection response of all beams shows a consistent increase in ultimate deflection with increasing concrete compressive strength. This indicates that increasing the compression zone capacity allows the beams to bear higher loads and undergo greater deformations before reaching the ultimate state. For beam 2B-4S, where the reaction to deformation was by steel yielding followed by concrete crushing at both concrete strengths, the ultimate deflection increased only slightly. This is due to the fact that the response of the beam is primarily controlled by steel reinforcement. While the higher concrete strength increased the load-carrying ability and slightly extended the deformation range, the ductility of the beams was maintained by steel yielding and there was limited increase in ultimate deflection. The deflection of beams 3B-3S and 4B-2S was significantly increased due to the increased BFRP stress at higher concrete strengths. Overall, increasing the concrete strength improves the load and deflection capacities of hybrid beams, but it does so depend on the type of reinforcement used.

6. SCOPE AND INTERPRETATIVE FRAMEWORK

The internal mechanical parameters reported in this paper, e.g., BFRP stress utilization and development of neutral axis are modeled predictions. While the FE model reproduces the global load-deflection response with high accuracy, the local strain and stress distributions are derived from the constituent laws of the CDP. These results are specific to the investigated beam geometry and reinforcement configuration. Therefore, trends in the numerical data should be interpreted as scientifically supported predictions to guide future experiments rather than empirically established local benchmarks.

7. CONCLUSIONS

Based on the detailed finite element analysis, experimental validation and parametric study presented in this paper, the following conclusions can be drawn:

1. The three-dimensional nonlinear finite element model developed in ABAQUS using the Concrete Damaged Plasticity (CDP) model demonstrated good accuracy in predicting ultimate load capacity, with an average error of 4.97%. This level of accuracy is well within the acceptable range for engineering applications and validates the CDP model and selected parameters for this class of structures, significantly reducing the need for costly trial-and-error experimental testing.
2. While the model adopts standard simplifications, such as idealized bond conditions and material homogeneity, which may lead to an underestimation of deflection in pure FRP members, it maintains high fidelity in capturing the interaction between steel yielding and concrete crushing in hybrid systems. These results confirm that the model can be reliably used as a computational tool for evaluating the synergy between high-strength concrete and hybrid reinforcement.
3. The structural response of hybrid beams is governed by the interaction between reinforcement type and concrete compressive strength. steel-dominant beams exhibited ductile behavior while BFRP-dominant beams show increased stiffness and reduced ductility.
4. Increasing concrete compressive strength Significantly enhances structural Performance and enables more effective utilization of BFRP tensile capacity, with the magnitude of increase strongly correlated with the BFRP reinforcement ratio.
5. The BFRP Stress Utilization Ratio (U_f) is predicted to increase significantly from approximately 60-70% in the reference beams to nearly full utilization (~99%) when concrete strength was enhanced to 120 MPa, suggesting that concrete strength is a critical factor in maximizing BFRP efficiency, as indicated by the numerical trends.
6. A transition in Failure mode was numerically observed with increasing concrete strength, shifting from concrete crushing toward BFRP-dominated behavior.
7. The findings regarding stiffness degradation provide critical data for the serviceability limit state design of structures subjected to repeated loads. BFRP-dominant hybrids, when coupled with 120 MPa concrete, offer superior long-term integrity and reduced maintenance requirements compared to conventional systems.

8. From a design perspective, achieving high BFRP utilization without reaching rupture is essential to ensure a safe and controlled failure mechanism. Therefore, an optimal balance between concrete strength and reinforcement ratio is required.
9. The results suggest a clear guideline for practitioners: steel-dominant hybrid configurations should be prioritized for seismic-prone areas requiring high energy dissipation, whereas BFRP-dominant configurations with ultra-high-strength concrete are optimal for maximizing load-carrying capacity in heavy-duty structural applications within the scope of the investigated parameters.

Acknowledgments

The authors gratefully acknowledge the support provided by the Civil Engineering Department at Mustansiriyah University for providing the laboratory facilities and equipment for this research. The authors also thank the technical staff for their assistance during the experimental program.

Credit Authorship Contribution Statement

Shahad Jawad Kadhim: Conceptualization, Methodology, Investigation, Data curation, Formal analysis, Writing – original draft. Hassan Falah Hassan: Supervision, Conceptualization, Methodology, Writing – review & editing.

Declaration of Competing Interest

The authors declare that they have no known competing financial interests or personal relationships that could have appeared to influence the work reported in this paper.

REFERENCES

Abed, F., Al-Mimar, M., and Ahmed, S., 2021. Performance of BFRP RC beams using high strength concrete. *Composites Part C: Open Access*, 4, 100107. https://doi.org/10.1016/j.jcomc.2021.100107

Abdulrahman, B.Q., 2025. Computational challenges and experimental validation of the flexural behaviour of RC beams using the nonlinear 3D finite element analysis by the damage plasticity model in Abaqus: A guidance study. *Russian Journal of Building Construction and Architecture*, 65(1), pp. 7–20. https://doi.org/10.36622/2542-0526.2025.65.1.001

ACI Committee 211, 2008. Guide for Selecting Proportions for High-Strength Concrete with Portland Cement and Fly Ash (ACI 211.4R-08). American Concrete Institute.

ACI Committee 440, 2015. Guide for the Design and Construction of Concrete Reinforced with FRP Bars (ACI 440.1R-15). American Concrete Institute.

ACI Committee 440, 2022. Building Code Requirements for Structural Concrete Reinforced with Glass Fiber-Reinforced Polymer (GFRP) Bars (ACI 440.11-22) and Commentary. American Concrete Institute.

Alkhteeb, L., and Dawood, M.B., 2025. Structural behavior of recycled aggregate concrete continuous beam with hybrid reinforcement under monotonic and repeated Load. *Revue des Composites et des Materiaux Avances*, 35(3), pp. 437–450. https://doi.org/10.18280/rcma.350305

Al-Shaarbaf, I.A.S., Ali, A.S., and Abdulridha, A.J., 2017. Experimental and numerical investigation of high strength reinforced concrete deep beams with web openings under repeated loading. *Al-*

Nahrain Journal for Engineering Sciences, 20(2), pp. 311–325. https://api.semanticscholar.org/CorpusID:114738693

Al-Zahrani, M.M., Mostafa, O.M., Rahman, M.K., and Najmuddin, S.K., 2023. Experimental and numerical investigations of BFRP-Reinforced normal and high strength concrete beams. *In: Ilki, A., Çavunt, D., and Çavunt, Y.S. (eds). Building for the Future: Durable, Sustainable, Resilient. fib Symposium 2023*. Lecture Notes in Civil Engineering, 349. Springer, Cham. https://doi.org/10.1007/978-3-031-32519-9_117

Assi, D., 2025. Non-linear finite element analysis for the verification and parametric study of reinforced concrete beams strengthened in compression zone to improve ductility by using ABAQUS. *Engineering and Technology Journal*, 43, pp. 401–410. https://doi.org/10.30684/etj.2025.157317.1912

ASTM C1240, 2015. Standard Specification for Silica Fume Used in Cementitious Mixtures. American Society for Testing and Materials.

ASTM C494/C494M, 2019. Standard Specification for Chemical Admixtures for Concrete. American Society for Testing and Materials.

Aziz, H.M, and Hassan, F.H., 2025. Structural Behavior of High-Strength Concrete Beams with Hybrid Reinforcement. MSc. Thesis, Department of Civil Engineering, College of Engineering, Al-Mustansiriyah University, Baghdad, Iraq.

Bažant, Z.P., and Jirásek, M., 2002. Nonlocal integral formulations of plasticity and damage: Survey of progress. *Journal of Engineering Mechanics*, 128(11), pp. 1119–1149. https://doi.org/10.1061/(ASCE)0733-9399(2002)128:11(1119)

Elbawab, Y., Elbawab, Y., El Zoughby, Z., ElKadi, O., AbouZeid, M. and Sayed-Ahmed, E., 2025. Flexural testing of Steel-, GFRP-, BFRP-, and hybrid reinforced beams. *Polymers*. https://doi.org/10.3390/polym17152027

Flayyih, A.S.Z., Dawood, M.B., and Habeeb, G.M., 2020. Flexural Behavior of Reinforced Concrete Composite Continuous T-Beam with Hybrid Reinforcement under Repeated Load. PhD. Thesis, Department of Civil Engineering, College of Engineering, University of Babylon, Babylon, Iraq.

Hollaway, L.C., and Teng, J.G., 2008. *Strengthening and Rehabilitation of Civil Infrastructures Using Fibre-Reinforced Polymer (FRP) Composites*. Woodhead Publishing.

Hordijk, D.A., 1991. Local Approach to Fatigue of Concrete. PhD. Thesis, Delft University of Technology, Delft, The Netherlands.

Ineia, A., Pol, W.D.O., Braun, J.C.A. and da Silva Lopes, L., 2021. Barras de fibra de vidro, uma alternativa inovadora e suas potencialidades: revisão bibliográfica. *Tecno-Lógica*, 25(2), pp. 243-251. https://dx.doi.org/10.17058/tecnolog.v25i2.16214

Kadhim, S. J., and Hassan, H. F., 2026. Experimental study of flexural behavior of high-strength concrete beams with hybrid reinforcement under repeated loading. *Structural Concrete*. https://doi.org/10.1002/suco.70700

Kossakowski, P. G., and Wciślik, W., 2022. Fiber-reinforced polymer composites in the construction of bridges: Opportunities, problems and challenges. *Fibers*, 10(4). https://doi.org/10.3390/fib10040037

Lu, Z.-H., and Zhao, Y.-G., 2010. Empirical stress-strain model for unconfined high-strength concrete under uniaxial compression. *Journal of Materials in Civil Engineering*, 22, pp. 1181–1186. https://doi.org/10.1061/(ASCE)MT.1943-5533.0000095

Maheswaran, J., and Chellapandian, M., 2023. Quantitative assessment of strengthening strategies and design recommendations for the repair of corrosion-damaged reinforced concrete members. *Buildings*, 13(4), 1080. https://doi.org/10.3390/buildings13041080

Megahed, K., 2025. Predicting flexural strength of hybrid FRP-steel reinforced beams using symbolic regression and ML techniques. *Scientific Reports*. https://doi.org/10.1038/s41598-025-05775-7

Mohamed, O. A., Al Hawat, W., and Keshawarz, M. S., 2021. Durability and mechanical properties of concrete reinforced with basalt fiber-reinforced polymer (BFRP) bars: Towards sustainable infrastructure. *Polymers*, 13(9), 1402. https://doi.org/10.3390/polym13091402

Nguyen, P.D., Dang, V.H., and Vu, N.A., 2020. Performance of concrete beams reinforced with various ratios of hybrid GFRP/Steel bars. *Civil Engineering Journal*, 6, pp. 1652–1669. https://doi.org/10.28991/cej-2020-03091572

Ortiz, J.D., Dolati, S.S.K., Malla, P., Nanni, A., and Mehrabi, A., 2023. FRP-reinforced/strengthened concrete: State-of-the-art review on durability and mechanical effects. *Materials*, 16(5), 1990. https://doi.org/10.3390/ma16051990

Oyshi, M. T., Azad, H. K. M., and Rahman, M. Z., 2023. Durability of FRP bars under varying environmental factors and loading conditions. In: *FRP Composites in Civil Engineering*. https://doi.org/10.1016/B978-0-323-96020-5.00216-8

Rasheed, H.A., Nayal, R., and Melhem, H., 2004. Response prediction of concrete beams reinforced with FRP bars. *Composite Structures*, 65, pp. 193–204. https://doi.org/10.1016/j.compstruct.2003.10.016

Ren, Y., Wang, H., and Guan, Z. Z., 2023. Evaluation of the properties and applications of FRP bars and anchors: A review. *Reviews on Advanced Materials Science*, 22, 20220287. https://doi.org/10.1515/rams-2022-0287

Salem, M., and Issa, M.S., 2023. Nonlinear finite element analysis of high and ultra-high strength concrete beams reinforced with FRP bars. *HBRC Journal*, 19, pp. 15–31. https://doi.org/10.1080/16874048.2023.2170765

Tatar, J., and Milev, S., 2021. Durability of externally bonded fiber-reinforced polymer composites in concrete structures: A critical review. *Polymers*, 13(5), 765. https://doi.org/10.3390/polym13050765

Thomas, M., 2013. Supplementary cementing materials in concrete. CRC Press, pp. 1–181. https://doi.org/10.1201/b14493

Tran, H., Nguyen-Thoi, T., and Dinh, H.B., 2025. State-of-the-art review of studies on the flexural behavior and design of FRP-Reinforced concrete beams. *Materials*, 18(14), 3295. https://doi.org/10.3390/ma18143295

Xie, Y., Zhuo, K., Rashid, K., Deng, J., and Zhang, F., 2022. Flexural performance of BFRP bar reinforced high-strength concrete beam. *In: Ilki, A., Ispir, M., and Inci, P. (eds). 10th International Conference on FRP Composites in Civil Engineering (CICE 2021)*. Lecture Notes in Civil Engineering, 198. Springer, Cham. https://doi.org/10.1007/978-3-030-88166-5_9

Yan, D., and Wang, Q., 2025. Numerical simulation on structural behavior of FRP profile-concrete hybrid beams with bolt shear connector. *Structural Concrete*, 26, pp. 929–951. https://doi.org/10.1002/suco.202400877

Yu, T., Teng, J.G., Wong, Y.L., and Dong, S.L., 2010. Finite element modeling of confined concrete-ii: plastic-damage model. *Engineering Structures*, 32, pp. 680–691. https://doi.org/10.1016/j.engstruct.2009.11.013

Yun, X., and Gardner, L., 2017. Stress-strain curves for hot-rolled steels. *Journal of Constructional Steel Research*, 133, pp. 36–46. https://doi.org/10.1016/j.jcsr.2017.01.024

حساب العناصر المحدودة لأداء الانحناء في العوارض الخرسانية المسلحة الهجينة (الحديد-BFRP) تحت الأحمال المتكررة: التحقق والدراسة البارامترية

شهد جواد كاظم*، حسن فلاح حسن

قسم الهندسة المدنية، كلية الهندسة ،الجامعة المستنصرية، بغداد، العراق

الخلاصة

لا يزال تآكل قضبان الحديد في الهياكل الخرسانية المسلحة المعرضة لظروف بيئية قاسية يمثل تحديًا كبيرًا. وقد أجريت أبحاث حول مركبات البوليمر المقوى بالألياف (FRP) باعتبارها بدائل محتملة لتسليح الصلب. تتمتع قضبان البوليمر المقوى بألياف البازلت (BFRP) بقوة شد ومتانة واستدامة ممتازة، لكنها تتميز بمرونة خطية وتتعرض للكسر الهش. ستجمع التعزيزات الهجينة من قضبان الحديد وBFRP بين ليونة الحديد ومتانة BFRP. تقدم هذه الدراسة تطوير وتحقق نموذج العناصر المحدودة (FE) ثلاثي الأبعاد غير الخطي في ABAQUS لمحاكاة سلوك الانحناء لعوارض الخرسانة عالية القوة (HSC) المقواة بنظام تعزيز هجين (حديد/BFRP) تحت أحمال متكررة. تم نمذجة ست عينات من العوارض ذات قوة ضغط تبلغ 86.5 ميجا باسكال والتحقق من صحتها مقارنة بالنتائج التجريبية. تنبأ نموذج العناصر المحدودة بسعة الحمل القصوى بخطأ متوسط قدره 4.97٪، بينما أظهرت تنبؤات الانحراف خطأً متوسطًا قدره 17.44٪. فشلت العوارض عندما حصل تصدع في الخرسانة قبل أن تصل قضبان BFRP إلى سعة الشد الكاملة. بحثت دراسة بارامترية في آثار زيادة قوة ضغط الخرسانة من 86.5 ميجا باسكال إلى 120 ميجا باسكال على إجهاد BFRP، وسعة الحمل القصوى، وطريقة الفشل. تشير النتائج إلى أن زيادة قوة الخرسانة إلى 120 ميجا باسكال تعزز الأداء الهيكلي بشكل كبير وتحسن استخدام BFRP. توفر هذه النتائج رؤى قيّمة حول تحسين أنظمة التسليح الهجينة من أجل تحسين الكفاءة الهيكلية والمتانة.

الكلمات المفتاحية: عوارض خرسانية عالية المقاومة، التسليح الهجين، التحميل المتكرر، ABAQUS، الدراسة البارامترية.